

Large-Scale Multi-Antenna Multi-Sine Wireless Power Transfer

Yang Huang, *Student Member, IEEE*, and Bruno Clerckx, *Member, IEEE*

Abstract—Wireless Power Transfer (WPT) is expected to be a technology reshaping the landscape of low-power applications such as the Internet of Things, radio frequency identification (RFID) networks, etc. Although there has been some progress towards multi-antenna multi-sine WPT design, the large-scale design of WPT, reminiscent of massive MIMO in communications, remains an open challenge. In this paper, we derive efficient multiuser algorithms based on a generalizable optimization framework, in order to design transmit sinewaves that maximize the weighted-sum/minimum rectenna output DC voltage. The study highlights the significant effect of the nonlinearity introduced by the rectification process on the design of waveforms in multiuser systems. Interestingly, in the single-user case, the optimal spatial domain beamforming, obtained prior to the frequency domain power allocation optimization, turns out to be maximum ratio combining (MRC). In contrast, in the general weighted sum criterion maximization problem, the spatial domain beamforming optimization and the frequency domain power allocation optimization are coupled. Assuming channel hardening, low-complexity algorithms are proposed based on asymptotic analysis, to maximize the two criteria. The structure of the asymptotically optimal spatial domain precoder can be found prior to the optimization. The performance of the proposed algorithms is evaluated. Numerical results confirm the inefficiency of the linear model-based design for the single and multi-user scenarios. It is also shown that as nonlinear model-based designs, the proposed algorithms can benefit from an increasing number of sinewaves.

Index Terms—Wireless power transfer, energy harvesting, nonlinear model, massive MIMO, convex optimization.

I. INTRODUCTION

Low-power applications such as the Internet of Things and radio frequency identification networks are expected to benefit from far-field wireless power transfer (WPT) systems [2], which convert the electromagnetic radiation energy transmitted through wireless channels into DC power by a rectenna.

Though circuit-level designs have been intensively studied in an effort to improve the RF-to-DC conversion efficiency of a rectifier, it has been recently reported in the RF literature that the efficiency is also a function of the input waveforms and can be significantly improved by multi-sine signals [2], [3]. To boost the energy transfer efficiency by waveform designs, progress has been made in smart power beaming [2] (not leveraging multi-sine signals) and spatially combined multi-sine signals [3]. The main limitation of those methods is not

only the lack of a systematic approach to design waveforms, but also the fact that they operate without channel state information (CSI) at the transmitter (CSIT), which in communications is usually used to turn multipath fading into a benefit for users. Interestingly, a methodology to optimize waveforms has been derived by [4], where CSIT is shown to be also very helpful to WPT¹. This study opens interesting perspectives for WPT where the transmission strategy is dynamically adapted as a function of the CSI so as to make the best use of the RF spectrum and the multiple antennas to maximize the output DC power.

One challenge in formulating the waveform design problem is that an analytical rectenna model has to be assumed. Although most off-the-shelf rectifier models in the microwave theory literature are able to provide insights into the accurate rectification process, non-closed forms or highly complex structures in these models [7], [8] make it hard to derive efficient algorithms for WPT. In contrast, [9] built a simplified model, which is popular in simultaneous wireless information and power transfer, by truncating the Taylor expansion of the Shockley diode equation to the 2nd-order term². In the model, the rectenna output DC current is directly proportional to the average input power. Therefore, the model is subsequently referred to as a *linear* model.

However, it was recently shown in [4] that the linear model is inaccurate in characterizing the performance behaviour of multi-sine signals. A more accurate model accounts for the nonlinearity of the rectifier through the higher order terms (≥ 4). To balance the accuracy and complexity of the optimization, [4] used a Taylor expansion truncated to the n_o th-order term ($n_o \geq 4$) and used it to optimize multi-sine waveforms for WPT. Interestingly, the nonlinear model leads to a completely different spectrum usage compared to the linear model. Indeed, while the linear model favours narrow-band transmission with all the power allocated to a single frequency, the nonlinear model favours a power allocation over multiple frequencies. In [4], circuit simulations validate the adopted model, highlight the inaccuracy of the linear model and confirm the superiority of optimized waveforms over various baselines. The scaling law for WPT revealed by [4] shows that the rectenna output DC current scales linearly with the number of sinewaves. This is reminiscent of massive MIMO in communications and sheds interest on a large-scale design for WPT. Unfortunately, the waveform optimization in

¹Attempts have been made to obtain CSI for WPT, e.g. [5], [6].

²It has been reported in RF literature that the 4th-order truncation is necessary for characterizing the basic diode rectification process [10].

A preliminary version has been presented in the IEEE International Workshop on Signal Processing Advances in Wireless Communications 2015 [1].

Y. Huang and B. Clerckx are with the Department of Electrical and Electronic Engineering, Imperial College London, London SW7 2AZ, United Kingdom (e-mail: {y.huang13, b.clerckx}@imperial.ac.uk). The work of Y. Huang was supported by CSC Imperial Scholarship. This work has been partially supported by the EPSRC of UK, under grant EP/P003885/1.

[4] leads to a posynomial maximization problem, which is solved by reversed geometric programming (GP). Due to the exponential complexity [11], reversed GP is highly complex for large-scale designs, although it can be applied to any order in the truncation models.

This paper studies the large-scale multi-antenna multi-sine WPT. To the authors' best knowledge, this is the first paper looking at efficient nonlinear model-based waveform optimizations for a large-scale WPT architecture. The paper studies not only low-complexity waveform optimization algorithms but also the effect of the nonlinearity introduced by the rectification process on waveform designs. The main contributions are listed as follows.

First, a novel analytical model characterizing the nonlinear rectification is derived, inspired by [12]. The dependent variable of the new model is the rectenna output DC voltage v_{out} , while that in [4] is the current. As a Taylor series-based model, it is truncated to the 4th-order term, since this truncation has been validated by circuit simulations [4]. Interestingly, multiplying this voltage model by a constant leads to the current model in [4]. They are equivalent in terms of optimization.

Second, we develop an optimization framework to address waveform designs involving the Taylor series-based 4th-order truncation model. The model in [4] leads to reversed GP. To avoid this, the RF signal model is converted into a generalizable compact expression: a real-valued function of complex vector variables. The compact expression is essentially a quartic function that in general still leads to NP-hard problems [13]–[15]. To make the problem tractable, we introduce auxiliary variables and exploit convex relaxations [14], such that the quartic objective can be reduced to a nonconvex quadratic constraint in an equivalent problem. Then, the nonconvex constraint is linearized, and the equivalent problem is iteratively approximated. Following this, a variety of convex optimization techniques (e.g. successive convex approximation (SCA) [16], rank reduction [17], [18], etc.) can be used to solve the approximate problem. The waveform optimization framework is derived for a single-user WPT and is then generalized to multi-user WPT systems.

Third, assuming perfect CSIT, we propose waveform optimization algorithms to maximize the multi-user weighted sum v_{out} . We reveal that in the single-user case, the optimal spatial domain beamforming turns out to be maximum ratio combining (MRC). Hence, only the power allocation across frequencies needs to be optimized by an algorithm. The comparison of this single-user waveform design and the linear model-based design again confirms the inefficiency of the linear model [4]. In contrast, in the general multi-user scenario, we show that the power allocation across frequencies affects the optimal spatial domain beamforming, due to the nonlinear rectification. Hence, an algorithm is proposed to optimize both the spatial domain beamforming and the power allocation across frequencies. In the presence of more antennas and sinewaves, a channel hardening-exploiting algorithm is proposed, assuming that channel hardening happens among the spatial domain channel vectors across users and frequencies. It is revealed that the asymptotically optimal spatial domain

precoder is a linear combination of the users' spatial domain channels. Hence, the algorithms optimize power allocation across frequencies and users. As a nonlinear model-based design, the frequency domain power optimization can benefit from an increasing number of sinewaves.

Fourth, for the sake of fairness among users, we propose waveform optimization algorithms to maximize the minimum v_{out} . In the presence of a large number of antennas and sinewaves, we also propose channel hardening-exploiting algorithms. We show that the minimum v_{out} achieved by these fairness-aware algorithms can be improved by increasing the number of sinewaves.

Organization: Section II discusses the system model. Section III optimizes waveform for a single user. Sections IV and V respectively maximize the weighted-sum/minimum v_{out} . Section VI evaluates the performance. Conclusions are drawn in Section VII.

Notations: Matrices and vectors are in bold capital and bold lower cases, respectively. The notations $(\cdot)^T$, $(\cdot)^*$, $(\cdot)^*$, $(\cdot)^H$, $\text{Tr}\{\cdot\}$, $\|\cdot\|$, $\|\cdot\|_F$ and $|\cdot|$ represent the transpose, optimal solution, conjugate, conjugate transpose, trace, 2-norm, Frobenius norm and absolute value, respectively. The notation $\mathbf{A} \succeq 0$ means that \mathbf{A} is positive-semidefinite.

II. SYSTEM MODEL

A. Signal Transmission through Wireless Channels

In the considered WPT system, a M -antenna base station (BS), or known as power beacon, serves K single-antenna users (or rectennas) by delivering multi-sine energy signals over N frequencies. It is assumed that all spatial/frequency domain channel gains remain constant during the transmission, and the BS has perfect CSIT. The complex scalar channel gain between the m th antenna and the user q (for $q = 1, \dots, K$) at the n th frequency is designated as $h_{q,(n-1)M+m}$ (for $n = 1, \dots, N$ and $m = 1, \dots, M$), which is collected into $\mathbf{h}_q \in \mathbb{C}^{MN \times 1}$. Hence, $\mathbf{h}_q = [\mathbf{h}_{q,1}^T, \dots, \mathbf{h}_{q,N}^T]^T$, where $\mathbf{h}_{q,n} = [h_{q,(n-1)M+1}, \dots, h_{q,(n-1)M+M}]^T$ describes the spatial domain channel gains at the n th frequency.

By collecting the magnitude and the phase of the RF complex signal at angular frequency ω_n into a complex variable $s_{(n-1)M+m}$, the complex version of the signal transmitted by the m th BS antenna can be formulated as $\tilde{x}_m(t) \triangleq \sum_{n=1}^N s_{(n-1)M+m} e^{j\omega_n t}$. Hence, the RF signal transmitted by antenna m is $x_m(t) = \sqrt{2} \text{Re}\{\tilde{x}_m(t)\}$. The variable $s_{(n-1)M+m}$ is collected into $\mathbf{s} \in \mathbb{C}^{MN \times 1}$, such that $\mathbf{s} = [\mathbf{s}_1^T, \dots, \mathbf{s}_N^T]^T$ and $\mathbf{s}_n = [s_{(n-1)M+1}, \dots, s_{(n-1)M+M}]^T$ which characterizes the signals transmitted at angular frequency ω_n . Note that $\omega_n = \omega_1 + (n-1)\Delta\omega$, for $n = 1, \dots, N$ and $\omega_1 > (N-1)\Delta\omega/2$. Suppose that the BS transmit power is constrained by P , such that $\|\mathbf{s}\|^2 = \sum_{n=1}^N \sum_{m=1}^M |s_{(n-1)M+m}|^2 \leq P$. The complex RF signal through the channel between the m th transmit antenna and the q th user can be written as

$$\tilde{y}_{q,m}(t) = \sum_{n=1}^N s_{(n-1)M+m} h_{q,(n-1)M+m} e^{j\omega_n t}. \quad (1)$$

Hence, the RF signal input into the antenna at user q is

$$y_q(t) = \sqrt{2} \text{Re}\{\tilde{y}_q(t)\} = \sqrt{2} \text{Re}\left\{\sum_{m=1}^M \tilde{y}_{q,m}(t)\right\}. \quad (2)$$

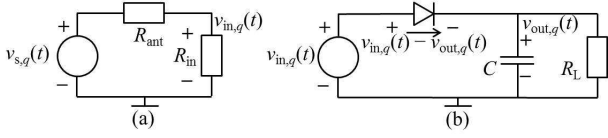


Fig. 1. (a) Antenna equivalent circuit. (b) Rectifier with a single-series diode. The capacitor C functions as a low-pass filter, and R_L is the load.

B. The Nonlinear Rectifying Process

1) *The Input Voltage of the Rectifier:* As shown in Fig. 1(a), the antenna at user q is modeled as a source $v_{s,q}(t)$ in series with an impedance $R_{ant} = 50\Omega$. Assuming a lossless antenna, all the input power to the rectenna can be absorbed by the rectifier's input impedance R_{in} , such that $\mathcal{E}\{|v_{in,q}(t)|^2\}/R_{in} = \mathcal{E}\{|y_q(t)|^2\}$. Maximizing the power dissipated in R_{in} yields $R_{ant} = R_{in}$. Assuming an ideal matching network, $v_{s,q}(t) = 2y_q(t)\sqrt{R_{ant}}$, and the rectifier input voltage is obtained as

$$v_{in,q}(t) = y_q(t)\sqrt{R_{ant}}, \quad (3)$$

2) *The Output Voltage of the Rectifier:* As shown in Fig. 1(b), the input signal is rectified by a Schottky diode and goes through a low pass filter. Inspired by [12], we then formulate the output voltage $v_{out,q}(t)$ as a function of input waveforms, by manipulating the Shockley diode equation.

The Shockley equation describes the instantaneous diode current $i_{d,q}(t)$ as a function of the voltage across the diode:

$$i_{d,q}(t) = i_s \left[\exp\left(\frac{v_{in,q}(t) - v_{out,q}(t)}{nV_T}\right) - 1 \right], \quad (4)$$

where i_s , V_T and n represent the saturation current, the thermal voltage and the ideality factor (set to 1 for simplicity), respectively. We consider that $i_{d,q}(t)$ is input into an ideal low pass filter $f_{LPF}(\cdot)$, where the non-DC components are removed and the power gain in the passband is 0 dB. Therefore, $v_{out,q}(t)$ in (4) yields a DC voltage, i.e. $v_{out,q}(t) = v_{out,q}$, and

$$i_{dc,q} = f_{LPF}(i_{d,q}(t)) = i_s e^{-\frac{v_{out,q}}{nV_T}} \cdot f_{LPF}\left(e^{\frac{v_{in,q}(t)}{nV_T}}\right) - i_s. \quad (5)$$

Due to the low-power input and the high impedance load, $i_{dc,q}$ in (5) is approximated to zero [12], such that $v_{out,q}$ can be written as a function of $v_{in,q}(t)$. Eq. (5) highlights that the nonlinear behavior of the diode comes from the term $\exp(\frac{v_{in,q}(t)}{nV_T})$. In order to obtain a tractable analytical model, this term is addressed by the small-signal analysis method: we apply Taylor expansion to this term (where $\frac{v_{in,q}(t)}{nV_T}$ is regarded as a whole) at 0 quiescent point. As it is revealed in the RF literature [10] and the waveform design [4] that the 4th-order truncation is necessary for characterizing the basic rectification, we truncate the Taylor series to the 4th-order term. Therefore,

$$v_{out,q} = nV_T \ln \left[1 + \frac{f_{LPF}(v_{in,q}^2(t))}{2n^2V_T^2} + \frac{f_{LPF}(v_{in,q}^4(t))}{24n^4V_T^4} \right], \quad (6)$$

where the odd order terms $f_{LPF}(v_{in,q}(t))/(nV_T)$ and $f_{LPF}(v_{in,q}^3(t))/(6n^3V_T^3)$ vanish and are removed, due to the fact that the odd order terms do not contribute to the DC voltage. We then make use of $\ln(1+x) \simeq x$ and combine (6)

$$\mathbf{M}_{q,1} = \begin{pmatrix} \mathbf{h}_{q,1}^* \mathbf{h}_{q,1}^T & \mathbf{h}_{q,1}^* \mathbf{h}_{q,2}^T & \mathbf{h}_{q,1}^* \mathbf{h}_{q,3}^T & \cdots & \mathbf{h}_{q,1}^* \mathbf{h}_{q,N}^T \\ \mathbf{h}_{q,2}^* \mathbf{h}_{q,1}^T & \mathbf{h}_{q,2}^* \mathbf{h}_{q,2}^T & \mathbf{h}_{q,2}^* \mathbf{h}_{q,3}^T & \cdots & \mathbf{h}_{q,2}^* \mathbf{h}_{q,N}^T \\ \mathbf{h}_{q,3}^* \mathbf{h}_{q,1}^T & \mathbf{h}_{q,3}^* \mathbf{h}_{q,2}^T & \mathbf{h}_{q,3}^* \mathbf{h}_{q,3}^T & \cdots & \mathbf{h}_{q,3}^* \mathbf{h}_{q,N}^T \\ \vdots & \vdots & \vdots & \ddots & \vdots \\ \mathbf{h}_{q,N}^* \mathbf{h}_{q,1}^T & \cdots & \cdots & \cdots & \mathbf{h}_{q,N}^* \mathbf{h}_{q,N}^T \end{pmatrix} \begin{matrix} \leftarrow k=1 \\ \leftarrow k=0 \end{matrix}$$

Fig. 2. $\mathbf{M}_{q,1}$ is the above matrix only maintaining the block diagonal (whose index is $k=1$) in pink, while all the other blocks are set as $\mathbf{O}_{M \times M}$.

and (3), achieving the rectifier output voltage as a function of the waveform input into the receive antenna:

$$v_{out,q} = \beta_2 f_{LPF}(y_q^2(t)) + \beta_4 f_{LPF}(y_q^4(t)), \quad (7)$$

where $\beta_2 = R_{ant}/(2nV_T)$ and $\beta_4 = R_{ant}^2/(24n^3V_T^3)$. Interestingly, multiplying the above $v_{out,q}$ by $i_s/(nV_T)$ achieves nothing else than the model z_{DC} (truncated to the 4th-order term) in [4]. Hence, the two models are equivalent in terms of optimization. Due to this and the fact that the model in [4] has been validated by circuit simulations, we do not conduct circuit simulations in this paper. The above model is built based on small signal analysis and valid only for the diode operating in the nonlinear region. If the input voltage is so large that the diode operates in the linear region, the assumptions made for approximation as well as the Taylor series-based model does not hold.

Then, $v_{out,q}$ can be expressed as a function of the transmit waveform, by combining (1), (2) and (7). In the term $f_{LPF}(y_q^2(t)) = f_{LPF}(\text{Re}\{\tilde{y}_q(t)\tilde{y}_q(t) + \tilde{y}_q(t)\tilde{y}_q^*(t)\})$, where $\text{Re}\{\tilde{y}_q(t)\tilde{y}_q(t)\}$ can be removed as it only contains the non-DC components. Hence,

$$f_{LPF}(y_q^2(t)) = \sum_{n=1}^N \sum_{m_1, m_2} [s_{(n-1)M+m_1} h_{q,(n-1)M+m_1} \cdot s_{(n-1)M+m_2}^* h_{q,(n-1)M+m_2}^*] = \sum_{n=1}^N \mathbf{s}_n^H \mathbf{h}_{q,n}^* \mathbf{h}_{q,n}^T \mathbf{s}_n, \quad (8)$$

where $m_1, m_2 \in \{1, \dots, M\}$. Similarly,

$$f_{LPF}(y_q^4(t)) = \frac{3}{2} f_{LPF}(\text{Re}\{\tilde{y}_q(t)\tilde{y}_q(t)\tilde{y}_q^*(t)\tilde{y}_q^*(t)\}) \quad (9a)$$

$$= \frac{3}{2} \sum_{\substack{n_1, n_2, n_3, n_4 \\ n_1+n_2=n_3+n_4}} \sum_{m_1, m_2, m_3, m_4} \left[\prod_{i=1}^2 s_{(n_i-1)M+m_i} h_{q,(n_i-1)M+m_i} \right]. \quad (9b)$$

$$= \frac{3}{2} \sum_{\substack{n_1, n_2, n_3, n_4 \\ n_1-n_3=-(n_2-n_4)}} \mathbf{s}_{n_3}^H \mathbf{h}_{q,n_3}^* \mathbf{h}_{q,n_1}^T \mathbf{s}_{n_1} \cdot \mathbf{s}_{n_4}^H \mathbf{h}_{q,n_4}^* \mathbf{h}_{q,n_2}^T \mathbf{s}_{n_2}, \quad (9c)$$

where $n_1, n_2, n_3, n_4 \in \{1, \dots, N\}$ and $m_1, m_2, m_3, m_4 \in \{1, \dots, M\}$. Substituting (8) and (9) into (7) yields

$$v_{out,q} = \beta_2 \sum_{n=1}^N \mathbf{s}_n^H \mathbf{h}_{q,n}^* \mathbf{h}_{q,n}^T \mathbf{s}_n + \frac{3}{2} \beta_4 \sum_{\substack{n_1, n_2, n_3, n_4 \\ n_1-n_3=-(n_2-n_4)}} \mathbf{s}_{n_3}^H \mathbf{h}_{q,n_3}^* \mathbf{h}_{q,n_1}^T \mathbf{s}_{n_1} \cdot \mathbf{s}_{n_4}^H \mathbf{h}_{q,n_4}^* \mathbf{h}_{q,n_2}^T \mathbf{s}_{n_2}. \quad (10)$$

3) *A compact expression*: The above (10) can be transformed into a more compact form, by introducing MN -by- MN matrices $\mathbf{M}_q \triangleq \mathbf{h}_q^* \mathbf{h}_q^T$ and $\mathbf{M}_{q,k}$. As shown in Fig. 2, $k \in \{1, \dots, N-1\}$ is the index of the k th block diagonal above the main block diagonal (whose index $k = 0$) of \mathbf{M}_q , while $k \in \{-(N-1), \dots, -1\}$ is the index of the $|k|$ th block diagonal below the main block diagonal. Given a certain k , $\mathbf{M}_{q,k}$ is generated by retaining the k th block diagonal of \mathbf{M}_q but setting all the other blocks as $\mathbf{0}_{M \times M}$. For $k \neq 0$, the non-Hermitian matrix $\mathbf{M}_{q,-k} = \mathbf{M}_{q,k}^H$, while $\mathbf{M}_{q,0} \succeq 0$. Hence, $v_{\text{out},q}$ can be written as

$$v_{\text{out},q} = \beta_2 \mathbf{s}^H \mathbf{M}_{q,0} \mathbf{s} + \frac{3}{2} \beta_4 \mathbf{s}^H \mathbf{M}_{q,0} \mathbf{s} (\mathbf{s}^H \mathbf{M}_{q,0} \mathbf{s})^H + 3\beta_4 \sum_{k=1}^{N-1} \mathbf{s}^H \mathbf{M}_{q,k} \mathbf{s} (\mathbf{s}^H \mathbf{M}_{q,k} \mathbf{s})^H. \quad (11)$$

This compact form cannot be generalized to a higher-order truncation model. For a higher-order truncation model, waveform optimizations have to be solved by reversed GP [4].

III. SINGLE-USER WAVEFORM OPTIMIZATION

A. A Frequency Domain Power Allocation Problem

To maximize the output DC voltage shown in (10) or (11) for a single-user (i.e. $K = 1$ and $q = 1$) WPT, the waveform optimization problem can be formulated as

$$\max_{\mathbf{s}} \{v_{\text{out},1} : \|\mathbf{s}\|^2 \leq P\}. \quad (12)$$

As defined in Section II-A, \mathbf{s} collects the spatial domain precoder across frequencies. Intuitively, finding an optimal \mathbf{s}^* for problem (12) amounts to optimizing both the normalized spatial domain beamforming and the power allocation across frequencies. The following theorem reveals that the optimal spatial domain beamforming for a single-user WPT is essentially MRC. This means that only the power allocation across frequencies would be optimized by an iterative algorithm.

Theorem 1: In problem (12), the optimal spatial domain precoder \mathbf{s}_n^* at frequency n has a structure of $\mathbf{s}_n^* \triangleq \xi_n^* \tilde{\mathbf{s}}_n^*$, where the optimal (normalized) spatial domain beamforming $\tilde{\mathbf{s}}_n^* = e^{j\phi_n} \mathbf{h}_{1,n}^* / \|\mathbf{h}_{1,n}\|$ and ξ_n^* is generally a complex weight.

Proof: Please refer to Appendix A for details. ■

Remark: Appendix A reveals that to maximize $v_{\text{out},1}$, though the optimal ξ_n^* and ϕ_n can be real and zero respectively as in [4], non-zero ϕ_n and complex ξ_n^* (meanwhile, $\xi_n^* e^{j\phi_n}$ is complex) can be found to achieve the same $v_{\text{out},1}$.

In the following, without loss of generality, we redefine $\mathbf{s}_n^* \triangleq \xi_n^* \cdot \mathbf{h}_{1,n}^* / \|\mathbf{h}_{1,n}\|$. Note that $|\xi_n|^2$ is the power allocated to the precoder \mathbf{s}_n at frequency n . Substituting the optimal structure of \mathbf{s}_n into (10) yields

$$v_{\text{out},1} = \beta_2 \sum_{n=1}^N |\xi_n|^2 \|\mathbf{h}_{1,n}\|^2 + \frac{3}{2} \beta_4 \sum_{\substack{n_1, n_2, n_3, n_4 \\ n_1 - n_3 = -(n_2 - n_4)}} \xi_{n_3}^* \|\mathbf{h}_{1,n_3}\| \cdot \|\mathbf{h}_{1,n_1}\| \xi_{n_1} \xi_{n_4}^* \|\mathbf{h}_{1,n_4}\| \|\mathbf{h}_{1,n_2}\| \xi_{n_2}. \quad (13)$$

Before formulating the optimization problem with respect to ξ_n , we formulate (13) in a more compact form. To the end, similarly to Section II-B3, we introduce N -by- N matrices \mathbf{M}_k'' and $\mathbf{M}'' \triangleq \mathbf{h}_{\text{norm}} \mathbf{h}_{\text{norm}}^T$, where $\mathbf{h}_{\text{norm}} = [\|\mathbf{h}_{1,1}\|, \dots, \|\mathbf{h}_{1,N}\|]^T$.

Given k , \mathbf{M}_k'' is generated by retaining the k th diagonal³ of \mathbf{M}'' but setting all the other entries as 0. Defining $\mathbf{p} \triangleq [\xi_1, \dots, \xi_N]^T$, (13) can be written as

$$v_{\text{out},1} = \beta_2 \mathbf{p}^H \mathbf{M}_0'' \mathbf{p} + \frac{3}{2} \beta_4 \mathbf{p}^H \mathbf{M}_0'' \mathbf{p} (\mathbf{p}^H \mathbf{M}_0'' \mathbf{p})^H + 3\beta_4 \sum_{k=1}^{N-1} \mathbf{p}^H \mathbf{M}_k'' \mathbf{p} (\mathbf{p}^H \mathbf{M}_k'' \mathbf{p})^H. \quad (14)$$

Hence, according to Theorem 1, problem (12) boils down to a frequency domain optimization problem, whose epigraph form can be formulated as

$$\min_{\gamma_0, \mathbf{p}} \gamma_0 \quad (15a)$$

$$\text{s.t. } -v_{\text{out},1}(\mathbf{p}) - \gamma_0 \leq 0, \quad (15b)$$

$$\mathbf{p}^H \mathbf{p} \leq P. \quad (15c)$$

The function $v_{\text{out},1}$ is a quartic polynomial, which in general makes problem (15) NP-hard [13]–[15]. To address the quartic polynomial, auxiliary variables t_k (for $k = 0, \dots, N-1$) are introduced, such that $\mathbf{p}^H \mathbf{M}_k'' \mathbf{p} = t_k$, and the quartic constraint (15b) can be reduced to a quadratic constraint. However, for $k \neq 0$, \mathbf{M}_k'' is not hermitian, and the term $\mathbf{p}^H \mathbf{M}_k'' \mathbf{p}$ is essentially a bilinear function, which may also lead to a NP-hard problem [19]. To handle this, a rank-1 matrix variable \mathbf{X} is introduced to linearize the bilinear term, such that $\mathbf{p}^H \mathbf{M}_k'' \mathbf{p} = \text{Tr}\{\mathbf{M}_k'' \mathbf{p} \mathbf{p}^H\} = \text{Tr}\{\mathbf{M}_k'' \mathbf{X}\} = t_k$. Then, defining $\mathbf{t} = [t_0, \dots, t_{N-1}]^T$,

$$\mathbf{A}_0 = \text{diag}\{-3\beta_4/2, -3\beta_4, \dots, -3\beta_4\} \preceq 0 \quad (16)$$

and $g(\mathbf{t}) \triangleq \mathbf{t}^H \mathbf{A}_0 \mathbf{t} = -3\beta_4 t_0 t_0^* / 2 - 3\beta_4 \sum_{k=1}^{N-1} t_k t_k^*$, problem (15) can be equivalently reformulated as

$$\min_{\gamma_0, \mathbf{t}, \mathbf{X} \succeq 0} \gamma_0 \quad (17a)$$

$$\text{s.t. } -\beta_2 t_0 + g(\mathbf{t}) - \gamma_0 \leq 0, \quad (17b)$$

$$\text{Tr}\{\mathbf{M}_k'' \mathbf{X}\} = t_k, \quad \forall k, \quad (17c)$$

$$\text{Tr}\{[\mathbf{M}_k'']^H \mathbf{X}\} = t_k^*, \quad \forall k \neq 0, \quad (17d)$$

$$\text{Tr}\{\mathbf{X}\} \leq P, \quad (17e)$$

$$\text{rank}\{\mathbf{X}\} = 1. \quad (17f)$$

B. Single-User Waveform Optimization Algorithm

Unfortunately, the nonconvex quadratic constraint (17b) and the rank constraint (17f) make problem (17) NP-hard in general. We first relax the rank constraint, solving

$$\min_{\gamma_0, \mathbf{t}, \mathbf{X} \succeq 0} \{\gamma_0 : (17b), (17c), (17d), \text{ and } (17e)\}. \quad (18)$$

By this means, solving problem (17) amounts to finding a rank-constrained \mathbf{X}^* of the relaxed problem (18).

³The subscript $k \in \{1, \dots, N-1\}$ in \mathbf{M}_k'' is the index of the k th diagonal above the main diagonal (whose index $k = 0$) of \mathbf{M}'' , while $k \in \{-(N-1), \dots, -1\}$ is the index of the $|k|$ th diagonal below the main diagonal.

Algorithm 1 SU WPT Algorithm

- 1: **Initialize** Set $l = 0$, and generate $\mathbf{X}^{(0)}$, $\mathbf{t}^{(0)}$ and $\gamma_0^{(0)}$;
 - 2: **repeat**
 - 3: $l = l + 1$;
 - 4: Compute \mathbf{A}_1'' ; $\mathbf{x}^* = \sqrt{P} [\mathbf{U}_{\mathbf{A}_1''}]_{\min}$; $\mathbf{X}^* = \mathbf{x}^*[\mathbf{x}^*]^H$;
 - 5: Update $\mathbf{X}^{(l)} = \mathbf{X}^*$; Update $t_k^{(l)} \forall k$ by (17c);
 - 6: **until** $\|\mathbf{X}^{(l)} - \mathbf{X}^{(l-1)}\|_F / \|\mathbf{X}^{(l)}\|_F \leq \epsilon$
 - 7: $\mathbf{p}^* = \mathbf{x}^*$ and $\mathbf{s}_n^* = [\mathbf{p}^*]_{n,1} \cdot \mathbf{h}_{1,n}^* / \|\mathbf{h}_{1,n}\|$ for $n = 1, \dots, N$.
-

1) *Solving the Relaxed Problem:* As problem (18) suffers from the nonconvex quadratic constraint (17b), the solution of (18) is approximated iteratively by SCA. At iteration l , the nonconvex term $g(\mathbf{t})$ in (17b) is approximated at $\mathbf{t}^{(l-1)}$, which is the optimal \mathbf{t}^* achieved at iteration $(l-1)$, as a linear function by its first-order Taylor expansion [20]

$$\tilde{g}(\mathbf{t}, \mathbf{t}^{(l-1)}) \triangleq 2\text{Re} \left\{ \left[\mathbf{t}^{(l-1)} \right]^H \mathbf{A}_0 \mathbf{t} \right\} - \left[\mathbf{t}^{(l-1)} \right]^H \mathbf{A}_0 \mathbf{t}^{(l-1)}. \quad (19)$$

Then, the l th approximate problem (AP) can be written as

$$\min_{\gamma_0, \mathbf{t}, \mathbf{X} \succeq 0} \gamma_0 \quad (20a)$$

$$\text{s.t.} \quad -\beta_2 t_0 + \tilde{g}(\mathbf{t}, \mathbf{t}^{(l-1)}) - \gamma_0 \leq 0, \quad (20b)$$

(17c), (17d), and (17e),

which is a semidefinite problem (SDP). Substituting (17c) and (17d) into (20b) shows that problem (20) is essentially equivalent to

$$\min_{\mathbf{X} \succeq 0} \{ \text{Tr}\{\mathbf{A}_1'' \mathbf{X}\} : \text{Tr}\{\mathbf{X}\} \leq P \}, \quad (21)$$

where $\mathbf{A}_1'' \triangleq \mathbf{C}_1'' + [\mathbf{C}_1'']^H$ is Hermitian, and

$$\mathbf{C}_1'' = -\frac{\beta_2 + 3\beta_4 t_0^{(l-1)}}{2} \mathbf{M}_0'' - 3\beta_4 \sum_{k=1}^{N-1} [t_k^{(l-1)}]^* \mathbf{M}_k'' \cdot \quad (22)$$

Applying [17, Proposition 3.5] shows that problem (21) has, among others, a rank-1 optimal solution \mathbf{X}^* . Due to the equivalence, this \mathbf{X}^* also satisfies the Karush-Kuhn-Tucker (KKT) conditions of (20). As (20) is convex, this \mathbf{X}^* is also a rank-1 global optimum of the AP (20).

2) *Achieving a Rank-1 \mathbf{X}^* of the AP:* To obtain a rank-1 solution \mathbf{X}^* in (20), if we solve the SDP (21) by the interior-point method and obtain the rank-1 solution by rank reduction [17, Algorithm 1], the complexity of solving the SDP is $O(1)(2+2N)^{1/2} N^2 (5N^4 + 8N^3 + N^2 + 1)$ [21]. Fortunately, the following method yields a closed-form solution, with reduced complexity.

Proposition 1: Problem (21) can yield, among others, a rank-1 optimal solution $\mathbf{X}^* = \mathbf{x}^*[\mathbf{x}^*]^H$, where $\mathbf{x}^* = \sqrt{P} [\mathbf{U}_{\mathbf{A}_1''}]_{\min}$ and $[\mathbf{U}_{\mathbf{A}_1''}]_{\min}$ is the eigenvector corresponding to the minimum eigenvalue of \mathbf{A}_1'' .

Proof: See Appendix B for details. ■

In order to achieve the rank-1 solution of Proposition 1, performing eigenvalue decomposition (EVD) for \mathbf{A}_1'' by the QR algorithm yields complexity of $O(N^3)$ [22]. The overall algorithm is summarized in Algorithm 1.

Theorem 2: If the eigenvectors of a given \mathbf{A}_1'' are uniquely attained, Algorithm 1 converges to a stationary point of problem (17).

Proof: As shown in [16, Theorem 1], the convergence of SCA is proved under the assumption that the minimizer converges to a limit point. However, theoretically, the eigenvectors of a given Hermitian matrix \mathbf{A}_1'' are not unique, and $\mathbf{X}^{(l)}$ in Algorithm 1 may not converge to a limit point. Therefore, similarly to [23] and [24], we establish the convergence under the condition that the eigenvectors of a given \mathbf{A}_1'' are uniquely attained. See Appendix C for the detailed proof. ■

IV. WEIGHTED SUM v_{OUT} MAXIMIZATION ALGORITHMS

A. Weighted Sum v_{out} Maximization

This subsection addresses the waveform optimization problem for a K -user system, aiming at maximizing the weighted sum output voltage. Defining $w_q \geq 0$ as the weight for user q , the problem can be formulated as

$$\max_{\mathbf{s}} \sum_{q=1}^K w_q \cdot v_{\text{out},q} \quad (23a)$$

$$\text{s.t.} \quad \|\mathbf{s}\|^2 \leq P. \quad (23b)$$

Remark : In contrast to the single-user problem (12), it is hard to find the optimal spatial domain beamforming for the K -user problem (23) prior to optimizing the frequency domain power allocation, due to the nonlinear rectification process. In the following, the intuition is revealed by a toy example. We first rewrite (23a) as

$$\sum_{q=1}^K w_q \cdot v_{\text{out},q} = \beta_2 \sum_{n=1}^N \mathbf{s}_n^H \left[\sum_{q=1}^K w_q \mathbf{h}_{q,n}^* \mathbf{h}_{q,n}^T \right] \mathbf{s}_n + \frac{3}{2} \beta_4 \cdot \sum_{\substack{n_1, n_2, n_3, n_4 \\ n_1 - n_3 = -(n_2 - n_4)}} \mathbf{s}_{n_3}^H \left[\sum_{q=1}^K w_q \mathbf{h}_{q,n_3}^* \mathbf{h}_{q,n_1}^T \mathbf{s}_{n_1} \mathbf{s}_{n_4}^H \mathbf{h}_{q,n_4}^* \mathbf{h}_{q,n_2}^T \right] \mathbf{s}_{n_2}. \quad (24)$$

As shown in (24), the 4th-order term (which is multiplied by β_4) is a sum of polynomials. The term is so complicated that we could not gain intuition from it. Therefore, we take the case of $N = 3$ as a toy example. Then, the polynomial in the 4th-order term with respect to $n_2 = n_3 = 1$ can be written as

$$f_{\beta_4} = \mathbf{s}_1^H \left[\sum_{q=1}^K w_q \mathbf{h}_{q,1}^* \left[\sum_{n=1}^3 \mathbf{h}_{q,n}^T \mathbf{s}_n \mathbf{s}_n^H \mathbf{h}_{q,n}^* \right] \mathbf{h}_{q,1}^T \right] \mathbf{s}_1. \quad (25)$$

Define $\mathbf{s}_n \triangleq \xi_n \tilde{\mathbf{s}}_n$, where $\tilde{\mathbf{s}}_n$ represents the spatial domain beamforming, and ξ_n is a complex weight related to the frequency domain power allocation. Given $\tilde{\mathbf{s}}_2$ and $\tilde{\mathbf{s}}_3$, if we would like to find the optimal $\tilde{\mathbf{s}}_1^*$ that maximizes (25), the problem can be formulated as

$$\arg \max_{\tilde{\mathbf{s}}_1} \mathbf{s}_1^H \left[\sum_{q=1}^K w_q \mathbf{h}_{q,1}^* \left[\sum_{n=1}^3 |\xi_n|^2 |\theta_{q,n}|^2 \right] \mathbf{h}_{q,1}^T \right] \mathbf{s}_1, \quad (26)$$

where $\theta_{q,n} \triangleq \mathbf{h}_{q,n}^T \tilde{\mathbf{s}}_n$. It can be seen that in the single-user case i.e. $K = 1$, the optimal $\tilde{\mathbf{s}}_1^*$ is MRC. However, when $K > 1$, as $|\xi_n|^2$ is coupled with $|\theta_{q,n}|^2$, the frequency domain power allocation affects the optimal structure of $\tilde{\mathbf{s}}_1$.

Therefore, we directly optimize \mathbf{s} for problem (23). The quartic $v_{\text{out},q} \forall q$ are tackled by introducing auxiliary variables in the same way as we transform (15) into (17). Defining

Algorithm 2 Weighted Sum (WSum) Algorithm

- 1: **Initialize** Set $l = 0$, and generate $\mathbf{X}^{(0)}$, $\{\mathbf{t}_q^{(0)}\}_{q=1}^K$;
 - 2: **repeat**
 - 3: $l = l + 1$;
 - 4: Compute \mathbf{A}_1 ; $\mathbf{x}^* = \sqrt{P}[\mathbf{U}_{\mathbf{A}_1}]_{\min}$; $\mathbf{X}^* = \mathbf{x}^*[\mathbf{x}^*]^H$;
 - 5: Update $\mathbf{X}^{(l)} = \mathbf{X}^*$; Update $t_{q,k}^{(l)} \forall q, k$ by (27c);
 - 6: **until** $\|\mathbf{X}^{(l)} - \mathbf{X}^{(l-1)}\|_F / \|\mathbf{X}^{(l)}\|_F \leq \epsilon$
 - 7: $\mathbf{s}^* = \mathbf{x}^*$.
-

$\mathbf{t}_q \triangleq [t_{q,0}, \dots, t_{q,N-1}]^T$ and $g_q(\mathbf{t}_q) \triangleq \mathbf{t}_q^H \mathbf{A}_0 \mathbf{t}_q$ (where \mathbf{A}_0 is defined in (16)), problem (23) can be equivalently recast as

$$\min_{\gamma_1, \{\mathbf{t}_q\}_{q=1}^K, \mathbf{X} \succeq 0} \gamma_1 \quad (27a)$$

$$\text{s.t.} \quad \sum_{q=1}^K w_q (-\beta_2 t_{q,0} + g_q(\mathbf{t}_q)) - \gamma_1 \leq 0, \quad (27b)$$

$$\text{Tr}\{\mathbf{M}_{q,k} \mathbf{X}\} = t_{q,k}, \quad \forall q, k, \quad (27c)$$

$$\text{Tr}\{\mathbf{M}_{q,k}^H \mathbf{X}\} = t_{q,k}^*, \quad \forall q, k \neq 0, \quad (27d)$$

$$\text{Tr}\{\mathbf{X}\} \leq P, \quad (27e)$$

$$\text{rank}\{\mathbf{X}\} = 1. \quad (27f)$$

In order to solve (27), we apply the approach used in Section III-B1. That is, we relax the rank constraint and then solve the relaxed problem by SCA. Specifically, at iteration l , $g_q(\mathbf{t}_q)$ in (27b) can be approximated (or linearized) as

$$\tilde{g}_q(\mathbf{t}_q, \mathbf{t}_q^{(l-1)}) \triangleq 2\text{Re}\left\{ \left[\mathbf{t}_q^{(l-1)} \right]^H \mathbf{A}_0 \mathbf{t}_q \right\} - \left[\mathbf{t}_q^{(l-1)} \right]^H \mathbf{A}_0 \mathbf{t}_q^{(l-1)}. \quad (28)$$

Note that (28) has the property $\tilde{g}_q(\mathbf{t}_q^{(l)}, \mathbf{t}_q^{(l)}) = g_q(\mathbf{t}_q^{(l)}) \leq \tilde{g}_q(\mathbf{t}_q^{(l)}, \mathbf{t}_q^{(l-1)})$. Then, the l th convex AP can be obtained as

$$\min_{\gamma_1, \{\mathbf{t}_q\}_{q=1}^K, \mathbf{X} \succeq 0} \gamma_1 \quad (29a)$$

$$\text{s.t.} \quad \sum_{q=1}^K w_q \left(-\beta_2 t_{q,0} + \tilde{g}_q(\mathbf{t}_q, \mathbf{t}_q^{(l-1)}) \right) \leq \gamma_1, \quad (29b)$$

(27c), (27d), and (27e),

which is equivalent to

$$\min_{\mathbf{X} \succeq 0} \{ \text{Tr}\{\mathbf{A}_1 \mathbf{X}\} : \text{Tr}\{\mathbf{X}\} \leq P \}, \quad (30)$$

where $\mathbf{A}_1 \triangleq \mathbf{C}_1 + \mathbf{C}_1^H$ and $\mathbf{C}_1 = \sum_{q=1}^K w_q \left(-\frac{\beta_2 + 3\beta_4 t_{q,0}^{(l-1)}}{2} \mathbf{M}_{q,0} - 3\beta_4 \sum_{k=1}^{N-1} t_{q,k}^{(l-1)} \mathbf{M}_{q,k} \right)$. According to Proposition 1, problem (30) can yield a rank-1 solution. The algorithm is summarized in Algorithm 2, where performing EVD for \mathbf{A}_1 can have complexity of $O((MN)^3)$. Similarly to Theorem 2, it can be shown that if the eigenvectors of a given \mathbf{A}_1 are uniquely attained, Algorithm 2 converges to a stationary point of problem (27).

B. Simplified Weighted Sum v_{out} Maximization

This subsection proposes a simplified K -user weighted sum v_{out} algorithm, where the spatial domain beamforming is obtained in a closed form, based on a linear model. Specifically, the linear model with respect to the K -user weighted sum v_{out} can be formulated as the 2nd-order truncation of (24), i.e. the term in (24) multiplied by β_2 . Considering this linear model, in order to maximize the weighted sum criterion, the optimal spatial domain beamforming \mathbf{w}_n (for $\|\mathbf{w}_n\| = 1$) is shown to be the dominant eigenvector of $\sum_{q=1}^K w_q \mathbf{h}_{q,n}^* \mathbf{h}_{q,n}^T$.

Then, considering such a *linear model*-based spatial domain beamforming design, the frequency domain power allocation is optimized based on the *nonlinear* model.

Given \mathbf{w}_n , the precoder at frequency n is $\mathbf{s}_n = \xi_n \mathbf{w}_n$, for $\xi_n \in \mathbb{C}$. Similarly to (14), we write $v_{\text{out},q}$ as a function of ξ_n in a compact form, by introducing matrices $\mathbf{M}_{q,k}''$ and $\mathbf{M}_{q,k}'''$. It is defined that $\mathbf{M}_{q,k}'' \triangleq \mathbf{h}_{e,q} \mathbf{h}_{e,q}^H$, where $\mathbf{h}_{e,q} \triangleq [\mathbf{w}_1^H \mathbf{h}_{q,1}^*, \dots, \mathbf{w}_N^H \mathbf{h}_{q,N}^*]^T$. Given k , $\mathbf{M}_{q,k}'''$ is generated by retaining the k th diagonal⁴ of $\mathbf{M}_{q,k}''$ but setting all the other entries as 0. Therefore, by defining $\mathbf{p} \triangleq [\xi_1, \dots, \xi_N]^T$, $v_{\text{out},q} = \beta_2 \mathbf{p}^H \mathbf{M}_{q,0}''' \mathbf{p} + \frac{3}{2} \beta_4 \mathbf{p}^H \mathbf{M}_{q,0}''' \mathbf{p} (\mathbf{p}^H \mathbf{M}_{q,0}''' \mathbf{p})^H + 3\beta_4 \sum_{k=1}^{N-1} \mathbf{p}^H \mathbf{M}_{q,k}''' \mathbf{p} (\mathbf{p}^H \mathbf{M}_{q,k}''' \mathbf{p})^H$. Then, the simplified weighted sum- v_{out} maximization problem $\max_{\mathbf{p}} \{ \sum_{q=1}^K w_q v_{\text{out},q}(\mathbf{p}) : \|\mathbf{p}\|^2 \leq P \}$ can be recast as

$$\min_{\gamma_1', \{\mathbf{t}_q\}_{q=1}^K, \mathbf{X} \succeq 0} \gamma_1' \quad (31a)$$

$$\text{s.t.} \quad \sum_{q=1}^K w_q (-\beta_2 t_{q,0} + g_q(\mathbf{t}_q)) - \gamma_1' \leq 0, \quad (31b)$$

$$\text{Tr}\{\mathbf{M}_{q,k}''' \mathbf{X}\} = t_{q,k}, \quad \forall q, k, \quad (31c)$$

$$\text{Tr}\{[\mathbf{M}_{q,k}''']^H \mathbf{X}\} = t_{q,k}^*, \quad \forall q, k \neq 0, \quad (31d)$$

$$\text{Tr}\{\mathbf{X}\} \leq P, \quad (31e)$$

$$\text{rank}\{\mathbf{X}\} = 1. \quad (31f)$$

It is shown that problem (31) has the same structure as problem (27). Hence, (31) can be solved by a variation of Algorithm 2. In order to apply Algorithm 2 to (31), changes are made as follows. The matrix \mathbf{A}_1 in Line 4 of Algorithm 2 should be replaced by $\mathbf{A}_1' \triangleq \mathbf{C}_1' + [\mathbf{C}_1']^H$, where $\mathbf{C}_1' = \sum_{q=1}^K w_q \left(-\frac{\beta_2 + 3\beta_4 t_{q,0}^{(l-1)}}{2} \mathbf{M}_{q,0}''' - 3\beta_4 \sum_{k=1}^{N-1} t_{q,k}^{(l-1)} \mathbf{M}_{q,k}''' \right)$. Line 4 of Algorithm 2 should be modified as $\mathbf{p}^* = \mathbf{x}^*$ and $\mathbf{s}_n^* = [\mathbf{p}^*]_{n,1} \mathbf{w}_n \forall n$. Due to space constraint, the algorithm is not outlined in pseudocode as Algorithm 2.

C. Exploiting Channel Hardening

This subsection proposes a channel hardening-exploiting (CHE) weighted sum v_{out} maximization algorithm, under the assumption that the channel of a given user is sufficiently frequency-selective such that channel gains can be i.i.d. in space and frequency. Additionally, the channels across users are fully uncorrelated. That is, given the large-scale fading $\Lambda_q^{1/2}$ and $h_{q,(n-1)M+1} \sim \mathcal{CN}(0, \Lambda_q)$, channel hardening indicates that as $M \rightarrow \infty$, $\mathbf{h}_{q,n}^T \mathbf{h}_{q,n}^* / M = \Lambda_q$ and $\mathbf{h}_{q,n}^T \mathbf{h}_{q',n'}^* / M = 0$ for $q' \neq q$ or $n' \neq n$.

1) *Asymptotical Analysis*: As defined in Section II-A, the spatial domain precoders across frequencies are collected in \mathbf{s} . In the following, the asymptotically optimal \mathbf{s} is referred to as \mathbf{s}_{asym} , of which the normalized version is designated as $\bar{\mathbf{s}} = [\bar{\mathbf{s}}_1^T, \dots, \bar{\mathbf{s}}_N^T]^T$. Hence, $\bar{\mathbf{s}}_n$ is subject to $\sum_{n=1}^N \|\bar{\mathbf{s}}_n\|^2 = 1$. Then, the optimal structure of $\bar{\mathbf{s}}_n$ can be

$$\bar{\mathbf{s}}_n = \sum_{q=1}^K \xi_{q,n} \mathbf{h}_{q,n}^* / \sqrt{M}, \quad (32)$$

⁴The subscript $k \in \{1, \dots, N-1\}$ in $\mathbf{M}_{q,k}'''$ is the index of the k th diagonal above the main diagonal (whose index $k = 0$) of $\mathbf{M}_{q,k}''$, while $k \in \{-(N-1), \dots, -1\}$ is the index of the $|k|$ th diagonal below the main diagonal.

where $\xi_{q,n}$ is a complex weight. With such a $\bar{\mathbf{s}}_n$, by defining $E \triangleq PM$, the asymptotically optimal⁵ \mathbf{s} can be written as

$$\mathbf{s}_{\text{asym}} \triangleq \sqrt{E/M\bar{\mathbf{s}}}. \quad (33)$$

Substituting \mathbf{s}_{asym} into (11) and exploiting channel hardening, the asymptotic output voltage at user q can be written as

$$v'_{\text{out},q} = \beta_2 E \Lambda_q^2 \mathbf{p}_q^H \mathbf{p}_q + \frac{3}{2} \beta_4 E^2 \Lambda_q^4 (\mathbf{p}_q^H \mathbf{M}'_0 \mathbf{p}_q) (\mathbf{p}_q^H \mathbf{M}'_0 \mathbf{p}_q)^H + 3\beta_4 E^2 \Lambda_q^4 \sum_{k=1}^{N-1} (\mathbf{p}_q^H \mathbf{M}'_k \mathbf{p}_q) (\mathbf{p}_q^H \mathbf{M}'_k \mathbf{p}_q)^H, \quad (34)$$

where $\mathbf{p}_q = [\xi_{q,1}, \dots, \xi_{q,N}]^T$. In (34), \mathbf{M}'_k returns a N -by- N matrix whose k th diagonal⁶ is made of ones, while all the other entries are zero. Assuming uniform power allocation across frequencies and considering the constraint on $\bar{\mathbf{s}}_n$, \mathbf{p}_1 can be written as $\mathbf{p}_1 = \frac{1}{\sqrt{N\Lambda_1}} \mathbf{1}_{N \times 1}$. Then, (34) becomes

$$v'_{\text{out},1} = \beta_2 E \Lambda_1 + 3\beta_4 E^2 \Lambda_1^2 / 2 + \beta_4 E^2 \Lambda_1^2 N(N-1)(2N-1)/(2N^2). \quad (35)$$

It is shown that if N is sufficiently large, $v'_{\text{out},q}$ linearly scales with N . This observation is in line with the scaling law of [4] for frequency-selective channels.

2) *Asymptotically Optimal Waveform Design*: The weighted sum v_{out} maximization problem can be formulated as

$$\max_{\{\mathbf{p}_q\}_{q=1}^K} \left\{ \sum_{q=1}^K w_q \cdot v'_{\text{out},q} : \sum_{q=1}^K \Lambda_q \|\mathbf{p}_q\|^2 = 1 \right\}. \quad (36)$$

Therefore, the algorithm to be derived from (36) optimizes power allocation across frequencies and users. Similarly to Section IV-A, in order to solve (36), it is reformulated as

$$\min_{\gamma'_1, \{\mathbf{p}_q\}_{q=1}^K, \{\mathbf{t}_q\}_{q=1}^K} \gamma'_1 \quad (37a)$$

$$\text{s.t.} \quad \sum_{q=1}^K w_q (E^2 \Lambda_q^4 g_q(\mathbf{t}_q) - \beta_2 E \Lambda_q^2 t_{q,0}) \leq \gamma'_1, \quad (37b)$$

$$\mathbf{p}_q^H \mathbf{M}'_k \mathbf{p}_q = t_{q,k}, \forall q, k \quad (37c)$$

$$\mathbf{p}_q^H [\mathbf{M}'_k]^H \mathbf{p}_q = t_{q,k}^*, \forall q, k \neq 0 \quad (37d)$$

$$\sum_{q=1}^K \Lambda_q \|\mathbf{p}_q\|^2 = 1, \quad (37e)$$

where $k=0, \dots, N-1$. To solve the problem, $g_q(\mathbf{t}_q)$ in (37b) is linearized by (28), yielding the AP of (37) at the l th iteration

$$\min_{\gamma'_1, \{\mathbf{p}_q\}_{q=1}^K, \{\mathbf{t}_q\}_{q=1}^K} \gamma'_1 \quad (38a)$$

$$\text{s.t.} \quad \sum_{q=1}^K w_q \left(-\beta_2 E \Lambda_q^2 t_{q,0} + E^2 \Lambda_q^4 \tilde{g}_q(\mathbf{t}_q, \mathbf{t}_q^{(l-1)}) \right) \leq \gamma'_1, \quad (38b)$$

(37c), (37d) and (37e).

Different from the APs (20) and (29), the AP (38) is nonconvex. Fortunately, the global optimum of (38) can be achieved by solving an equivalent problem. Substitute (37c) and (37d) into (37b). By defining

$$\mathbf{C}'_{q,1} \triangleq \frac{\beta_2 E \Lambda_q^2 + 3E^2 \Lambda_q^4 \beta_4 t_{q,0}^{(l-1)}}{2} \mathbf{M}'_0 - 3\beta_4 E^2 \Lambda_q^4 \sum_{k=1}^{N-1} [t_{q,k}^{(l-1)}]^* \mathbf{M}'_k \quad (39)$$

⁵The optimality of $\bar{\mathbf{s}}_n$ can be shown by contradiction as in [25]. Intuitively, if $\bar{\mathbf{s}}_n$ contains not only the linear combination of $\xi_{q,n} \mathbf{h}_{q,n}^*$ as in (32) but also the directions in the orthogonal complement of the space spanned by $\{\mathbf{h}_{q,n}\}_{q=1}^K$, some transmit power would not contribute to v_{out} and is wasted.

⁶For $k > 0$, k is the index of the k th diagonal above the main diagonal (whose index $k = 0$); for $k < 0$, k is the index of the $|k|$ th diagonal below the main diagonal. For instance, $\mathbf{M}'_0 = \mathbf{I}_{N \times N}$.

Algorithm 3 CHE WSum Algorithm

- 1: **Initialize** Set $l = 0$, and generate feasible initial points $\{\mathbf{p}_q^{(0)}\}_{q=1}^K$. Then, compute $\{\mathbf{t}_q^{(0)}\}_{q=1}^K$ by (37c).
- 2: **repeat**
- 3: $l = l + 1$;
- 4: Compute $\{\mathbf{C}'_{q,1}(\mathbf{t}_q^{(l-1)})\}_{q=1}^K$ and $\{\mathbf{A}'_{q,1}(\mathbf{t}_q^{(l-1)})\}_{q=1}^K$;
- 5: Compute $\mathbf{A}'_1, \bar{\mathbf{p}}^* = b[\mathbf{U}_{\bar{\Lambda}}]_{\min}$ and $\{\mathbf{p}_q^*\}_{q=1}^K$;
- 6: Update $\bar{\mathbf{p}}^{(l)} = \bar{\mathbf{p}}^*$ and $\mathbf{p}_q^{(l)} = \mathbf{p}_q^*, \forall q$; Update $t_{q,k}^{(l)}$;
- 7: **until** $\|\bar{\mathbf{p}}^{(l)} - \bar{\mathbf{p}}^{(l-1)}\| / \|\bar{\mathbf{p}}^{(l)}\| \leq \epsilon$
- 8: $\bar{\mathbf{s}}_n^* = \sum_{q=1}^K [\mathbf{p}_q^*]_n \mathbf{h}_{q,n} / \sqrt{M}$ and $\mathbf{s}_{\text{asym}}^* = \sqrt{E/M\bar{\mathbf{s}}^*}$

and

$$\mathbf{A}'_{q,1} \triangleq \mathbf{C}'_{q,1} + [\mathbf{C}'_{q,1}]^H, \quad (40)$$

the equivalent form of (38) can be formulated as

$$\min_{\bar{\mathbf{p}}} \left\{ \bar{\mathbf{p}}^H \mathbf{A}'_1 \bar{\mathbf{p}} : \bar{\mathbf{p}}^H \mathbf{\Lambda} \bar{\mathbf{p}} = 1 \right\}, \quad (41)$$

where $\bar{\mathbf{p}} \triangleq [\mathbf{p}_1^T, \dots, \mathbf{p}_K^T]^T$, $\mathbf{A}'_1 \triangleq \text{diag}\{w_1 \mathbf{A}'_{1,1}, \dots, w_K \mathbf{A}'_{K,1}\}$ and $\mathbf{\Lambda} \triangleq \text{diag}\{\mathbf{\Lambda}_1, \dots, \mathbf{\Lambda}_K\}$. All the main diagonal entries of the N -by- N diagonal matrix $\mathbf{\Lambda}_q$ are equal to Λ_q . Let $\mathbf{U}_{\bar{\Lambda}}$ collect the eigenvectors of $\bar{\Lambda} \triangleq \mathbf{\Lambda}^{-1} \mathbf{A}'_1$. Similarly to Proposition 1, the optimal $\bar{\mathbf{p}}^* = b[\mathbf{U}_{\bar{\Lambda}}]_{\min}$, where $b = [1/([\mathbf{U}_{\bar{\Lambda}}]_{\min}^H \mathbf{\Lambda} [\mathbf{U}_{\bar{\Lambda}}]_{\min})]^{1/2}$. For $\Lambda_q = \Lambda \forall q$, $\bar{\mathbf{p}}^* = \sqrt{\frac{1}{\Lambda}} [\mathbf{U}_{\mathbf{A}'_1}]_{\min}$, where $\mathbf{U}_{\mathbf{A}'_1}$ collects the eigenvectors of \mathbf{A}'_1 . Note that the EVD of $\bar{\Lambda}$ (or \mathbf{A}'_1) yields complexity of $O(KN^3)$. The algorithm is summarized in Algorithm 3. As (41) yields the global optimum of (38) and $\tilde{g}_q(\mathbf{t}_q^{(l)}, \mathbf{t}_q^{(l)}) = g_q(\mathbf{t}_q^{(l)}) \leq \tilde{g}_q(\mathbf{t}_q^{(l)}, \mathbf{t}_q^{(l-1)})$, the objective function of (38) decreases over iterations. Thus, Algorithm 3 finally converges to a stationary point of the original problem (37) provided the eigenvectors of a given $\bar{\Lambda}$ are uniquely attained.

V. MINIMUM v_{OUT} MAXIMIZATION ALGORITHMS

A. Minimum v_{out} Maximization

This subsection derives fairness-aware K -user waveform optimization algorithms, by maximizing the minimum v_{out} :

$$\max_{\mathbf{s}, \gamma_2} \{ \gamma_2 : v_{\text{out},q}(\mathbf{s}) \geq \gamma_2 \forall q, \|\mathbf{s}\|^2 \leq P \}. \quad (42)$$

For $K = 1$, (42) boils down to (12). To address the quartic polynomial $v_{\text{out},q}(\mathbf{s})$, auxiliary variables $t_{q,k}$ are introduced as in Section IV-A, such that (42) can be equivalently recast as

$$\min_{\gamma_2, \{\mathbf{t}_q\}_{q=1}^K, \mathbf{X} \succeq 0} -\gamma_2 \quad (43a)$$

$$\text{s.t.} \quad -\beta_2 t_{q,0} + g_q(\mathbf{t}_q) + \gamma_2 \leq 0, \forall q, \quad (43b)$$

$$\text{rank}\{\mathbf{X}\} = 1. \quad (43c)$$

(27c), (27d) and (27e).

Similarly to (27), (43) is nonconvex, due to the nonconvex (43b) and the rank constraint. To solve (43), we first relax the rank constraint, yielding

$$\min_{\gamma_2, \{\mathbf{t}_q\}_{q=1}^K, \mathbf{X} \succeq 0} -\gamma_2 \quad (44a)$$

$$\text{s.t.} \quad -\beta_2 t_{q,0} + g_q(\mathbf{t}_q) + \gamma_2 \leq 0, \forall q, \quad (44b)$$

(27c), (27d) and (27e).

Algorithm 4 Max-Min-RR Algorithm (for $K \leq 3$)

- 1: **Initialize** Set $l = 0$, and generate $\mathbf{X}^{(0)}$ and $\{\mathbf{t}_q^{(0)}\}_{q=1}^K$;
 - 2: **repeat**
 - 3: $l = l + 1$;
 - 4: Update \bar{c}_q , $\mathbf{C}_{q,1}$ and $\mathbf{A}_{q,1}$; solve problem (46) by the interior-point method, yielding a high-rank solution \mathbf{X}^* ;
 - 5: Find the optimal $q^* \triangleq q_0 = \arg \max_q \text{Tr}\{\mathbf{A}_{q,1}\mathbf{X}^*\} + \bar{c}_q$;
 - 6: Apply the RR procedure [17, Algorithm 1] to problem (48), yielding a rank-1 optimal solution $\mathbf{X}_{r1} = \mathbf{x}_0\mathbf{x}_0^H$;
 - 7: Update $\mathbf{X}^{(l)} = \mathbf{X}_{r1}$; update $\mathbf{t}_{q,k}^{(l)} \forall q, k$ by (27c);
 - 8: **until** $\|\mathbf{X}^{(l)} - \mathbf{X}^{(l-1)}\|_F / \|\mathbf{X}^{(l)}\|_F \leq \epsilon$
 - 9: $\mathbf{s}^* = \mathbf{x}_0$.
-

Therefore, achieving the solution of (43) amounts to finding a rank-constrained solution by solving (44). Problem (44) is nonconvex due to (44b). Therefore, we approximate the solution of (44) by SCA over iterations as in Section IV-A. Hence, by approximating (or linearizing) $g_q(\mathbf{t}_q)$ by (28), the AP of (44) at iteration l can be formulated as

$$\begin{aligned} \min_{\gamma_2, \{\mathbf{t}_q\}_{q=1}^K, \mathbf{X} \succeq 0} \quad & -\gamma_2 \\ \text{s.t.} \quad & -\beta_2 t_{q,0} + \tilde{g}_q(\mathbf{t}_q, \mathbf{t}_q^{(l-1)}) + \gamma_2 \leq 0, \forall q, \\ & (27c), (27d) \text{ and } (27e). \end{aligned} \quad (45a)$$

1) *Max-Min Algorithm with Rank Reduction (for $K \leq 3$):*

We first show that if $K \leq 3$, (45) can offer a solution with a rank-1 optimal \mathbf{X}_{r1} , although solving (45) by the interior-point method usually yields a solution with a *high-rank* \mathbf{X}^* [26]. Based on this, in order to solve (43), we then propose an algorithm based on SCA and a embedded rank reduction (RR) procedure, where the RR procedure is applied to the high-rank solution of the AP (45) to achieve a rank-1 \mathbf{X}_{r1} .

Theorem 3: Given $K \leq 3$, problem (45) can yield, among others, an optimal \mathbf{X}^* of rank 1.

Proof: Substituting (27c) and (27d) into (45a) and defining $\bar{c}_q = -[\mathbf{t}_q^{(l-1)}]^H \mathbf{A}_0 \mathbf{t}_q^{(l-1)}$, $\mathbf{C}_{q,1} = -\frac{\beta_2 + 3\beta_4 t_{q,0}^{(l-1)}}{2} \mathbf{M}_{q,0} - 3\beta_4 \sum_{k=1}^{N-1} [\mathbf{t}_{q,k}^{(l-1)}]^* \mathbf{M}_{q,k}$ and $\mathbf{A}_{q,1} = \mathbf{C}_{q,1} + \mathbf{C}_{q,1}^H$, problem (45) can be equivalently reformulated as

$$\min_{\gamma_2, \mathbf{X} \succeq 0} \{ -\gamma_2 : \text{Tr}\{\mathbf{A}_{q,1}\mathbf{X}\} + \bar{c}_q + \gamma_2 \leq 0 \forall q, \text{Tr}\{\mathbf{X}\} \leq P \}, \quad (46)$$

which can be transformed into another equivalent form:

$$\min_{\mathbf{X} \succeq 0} \max_{q=1 \dots K} \{ \text{Tr}\{\mathbf{A}_{q,1}\mathbf{X}\} + \bar{c}_q : \text{Tr}\{\mathbf{X}\} \leq P \}. \quad (47)$$

Given the optimal $q^* = q_0$ that maximizes $\text{Tr}\{\mathbf{A}_{q,1}\mathbf{X}\} + \bar{c}_q$, problem (47) boils down to

$$\min_{\mathbf{X} \succeq 0} \text{Tr}\{\mathbf{A}_{q_0,1}\mathbf{X}\} \quad (48a)$$

$$\text{s.t. } \text{Tr}\{(\mathbf{A}_{q,1} - \mathbf{A}_{q_0,1})\mathbf{X}\} \leq \bar{c}_{q_0} - \bar{c}_q, \forall q \neq q_0, \quad (48b)$$

$$\text{Tr}\{\mathbf{X}\} \leq P. \quad (48c)$$

In the case of $K \leq 3$, (48) turns out to be a separable SDP, and the number of its linear constraints is no greater than three. It can be shown that (48) can yield, among others, a rank-1 optimal solution [17, Proposition 3.5]. Therefore, for $K \leq 3$, problem (45) can yield a rank-1 \mathbf{X}_{r1} . ■

According to Theorem 3, for $K \leq 3$, Algorithm 4 is proposed to solve (43). In the algorithm, a rank-1 solution \mathbf{X}_{r1}

of (45) can be obtained by performing RR, such that solving (45) iteratively can finally make the solution $(\gamma_2, \{\mathbf{t}_q\}_{q=1}^K, \mathbf{X}_{r1})$ converge to a stationary point of (43). The proposed algorithm is elaborated and explained as follows.

Exploiting the interior-point method⁷ to solve (46), Line 4 of Algorithm 4 essentially solves the l th AP (45). As $\tilde{g}_q(\mathbf{t}_q^{(l)}, \mathbf{t}_q^{(l)}) = g_q(\mathbf{t}_q^{(l)}) \leq \tilde{g}_q(\mathbf{t}_q^{(l)}, \mathbf{t}_q^{(l-1)})$ and $\nabla g_q(\mathbf{t}_q^{(l)}) = \nabla \tilde{g}_q(\mathbf{t}_q^{(l)}, \mathbf{t}_q^{(l)})$, it can be shown that solving (45) iteratively can achieve a stationary point of (44). Intuitively, if the optimal \mathbf{X}^* of (45) always remains rank-1, the stationary point of (44) is also that of (43). According to Theorem 3, a RR procedure can be exploited to derive a rank-1 solution \mathbf{X}_{r1} from the high-rank solution of (45). To the end, Line 5 finds the optimal q^* , such that the parameters $\mathbf{A}_{q_0,1}$, $\mathbf{A}_{q,1} - \mathbf{A}_{q_0,1}$ and $\bar{c}_{q_0} - \bar{c}_q$ of problem (48) can be computed. Then, in Line 6, the RR procedure [17, Algorithm 1] is applied to problem (48) to obtain a rank-1 \mathbf{X}_{r1} , according to the proof of Theorem 3. Although the RR procedure [17, Algorithm 1] is iterative, the optimal q^* remains constant, as the values of $\text{Tr}\{\mathbf{X}\}$ and $\text{Tr}\{(\mathbf{A}_{q,1} - \mathbf{A}_{q_0,1})\mathbf{X}\}$ ($\forall q \neq q_0$) remain constant over iterations⁸. As the RR procedure preserves the primal feasibility and the complementary slackness of (48), the achieved \mathbf{X}_{r1} remains globally optimal for (48). Such a RR procedure is deterministic [18], namely, given $\mathbf{A}_{q,1}$, \bar{c}_q and P , the optimal rank-1 \mathbf{X}_{r1} is uniquely attained. Hence, similarly to Theorem 2, we can show that Algorithm 4 converges to a stationary point of (44). As the solution is rank-1, it is also a stationary point of (43).

2) *Max-Min Algorithm with Randomization (for an Arbitrary K):* It can be seen from the proof of Theorem 3 that when $K > 3$, problem (48) may not have a rank-1 optimal solution. Therefore, (44) cannot always yield a rank-1 optimal \mathbf{X}^* . Then, a SCA-then-randomization method is used to solve (43), such that a rank-1 \mathbf{X} can be achieved for (43).

Specifically, we exploit SCA to solve (44). To this end, we formulate the l th AP of (44) as (45). Problem (45) is iteratively solved by the interior-point method until convergence, yielding a high-rank solution \mathbf{X}^* , which is a stationary point of (44). In the following, a best feasible rank-1 solution \mathbf{X}_{r1}^* of (43) is derived from the high-rank \mathbf{X}^* . To the end, we first perform EVD $\mathbf{X}^* = \mathbf{U}_X \Sigma_X \mathbf{U}_X^H$. Following this, random vectors $\hat{\mathbf{x}}_t$ (for $t = 1, \dots, T$) are generated: $\hat{\mathbf{x}}_t = \mathbf{U}_X \Sigma_X^{1/2} \mathbf{v}_t$, where each complex entry in the random vector \mathbf{v}_t is drawn from a circular uniform distribution such that $\mathcal{E}\{\mathbf{v}_t \mathbf{v}_t^H\} = \mathbf{I}$. Then, T random rank-1 feasible solutions of (44) can be obtained by $\mathbf{X}_t = \hat{\mathbf{x}}_t \hat{\mathbf{x}}_t^H$. Thanks to the method for generating $\hat{\mathbf{x}}_t$, \mathbf{X}_t always satisfies the power constraint (27e). As $-\gamma_2$ is the objective function of (43) and thereby essentially a function of \mathbf{X} , we designate $-\gamma_2$ as $-\gamma_2(\mathbf{X})$. Therefore, the best feasible solution (in terms of \mathbf{X}) of (43) is $\mathbf{X}_{r1}^* = \arg \min_{\mathbf{X}_t} -\gamma_2(\mathbf{X}_t)$. Due to space constraint, the algorithm is not outlined in pseudocode.

⁷In our simulations, SDPs are solved by CVX. CVX invokes the universal solver SDPT3 to implement the interior-point algorithm [27].

⁸This is because the RR formula at Line 8 of [17, Algorithm 1] keeps the values of the constraint functions constant over iterations. See the proof of [17, Lemma 3.1] for details.

B. Exploiting Channel Hardening

Under the same assumption as in Section IV-C, this subsection proposes simplified algorithm for the minimum v_{out} maximization problem, by exploiting channel hardening. It can be shown that the structures of $\bar{\mathbf{s}}_n$ and \mathbf{s}_{asym} , i.e. (32) and (33), are still asymptotically optimal. With the asymptotic output voltage (34), the minimum v_{out} maximization problem can be formulated as $\max_{\{\mathbf{p}_q\}_{q=1}^K} \min_{q=1 \dots K} \{v'_{\text{out},q} : \sum_{q=1}^K \Lambda_q \|\mathbf{p}_q\|^2 = 1\}$, which can be equivalently recast as

$$\min_{\gamma'_2, \{\mathbf{p}_q\}_{q=1}^K, \{\mathbf{t}_q\}_{q=1}^K} -\gamma'_2 \quad (49a)$$

$$\text{s.t. } E^2 \Lambda_q g_q(\mathbf{t}_q) - \beta_2 E \Lambda_q^2 t_{q,0} + \gamma'_2 \leq 0, \forall q \quad (49b)$$

(37c), (37d) and (37e).

To solve (49), similarly to (37), $g_q(\mathbf{t}_q)$ in (49b) is linearized by (28), such that the l th AP of (49) can be formulated. Reusing the definitions (39) and (40), and defining

$$\bar{c}'_q = -[\mathbf{t}_q^{(l-1)}]^H \mathbf{A}_0 \mathbf{t}_q^{(l-1)} E^2 \Lambda_q^4, \quad (50)$$

the l th AP of (49) can be written as

$$\min_{\gamma'_2, \{\mathbf{p}_q\}_{q=1}^K} -\gamma'_2 \quad (51a)$$

$$\text{s.t. } \mathbf{p}_q^H \mathbf{A}'_{q,1} \mathbf{p}_q + \bar{c}'_q + \gamma'_2 \leq 0, \forall q \quad (51b)$$

$$\sum_{q=1}^K \Lambda_q \|\mathbf{p}_q\|^2 = 1, \quad (51c)$$

which is nonconvex. By introducing optimization variables $\mathbf{X}_q \triangleq \mathbf{p}_q \mathbf{p}_q^H \forall q$, a semidefinite relaxation (SDR) problem, where the constraints $\text{rank}\{\mathbf{X}_q\} = 1$ for $q = 1, \dots, K$ have been relaxed, can be formulated as

$$\min_{\gamma'_2, \{\mathbf{X}_q \succeq 0\}_{q=1}^K} -\gamma'_2 \quad (52a)$$

$$\text{s.t. } \text{Tr}\{\mathbf{A}'_{q,1} \mathbf{X}_q\} + \bar{c}'_q + \gamma'_2 \leq 0, \forall q, \quad (52b)$$

$$\sum_{q=1}^K \text{Tr}\{\Lambda_q \mathbf{I} \cdot \mathbf{X}_q\} = 1 \quad (52c)$$

or

$$\min_{\{\mathbf{X}_q \succeq 0\}_{q=1}^K} \max_{q=1 \dots K} \{\text{Tr}\{\mathbf{A}'_{q,1} \mathbf{X}_q\} + \bar{c}'_q : \sum_{q=1}^K \text{Tr}\{\Lambda_q \mathbf{I} \cdot \mathbf{X}_q\} = 1\}. \quad (53)$$

Hence, solving (51) boils down to obtaining the rank-constrained optimal $\{\mathbf{X}_q^*\}_{q=1}^K$ from (52) or (53).

Theorem 4: Problem (52) can yield rank-1 optimal \mathbf{X}_q in the presence of an arbitrary number of users.

Proof: The proof strategy is similar to that for Theorem 3. Given the optimal $q^* = q_0$ that maximizes $\text{Tr}\{\mathbf{A}'_{q,1} \mathbf{X}_q\} + \bar{c}'_q$, (53) can be reduced to

$$\min_{\{\mathbf{X}_q \succeq 0\}_{q=1}^K} \text{Tr}\{\mathbf{A}'_{q_0,1} \mathbf{X}_{q_0}\} + \bar{c}'_{q_0} \quad (54a)$$

$$\text{s.t. } \text{Tr}\{(\mathbf{A}'_{q,1} - \mathbf{A}'_{q_0,1}) \mathbf{X}_q\} \leq \bar{c}'_{q_0} - \bar{c}'_q, \forall q \neq q_0, \quad (54b)$$

$$\sum_{q=1}^K \text{Tr}\{\Lambda_q \mathbf{I} \cdot \mathbf{X}_q\} = 1. \quad (54c)$$

Problem (54) contains K linear constraints and K matrix variables. According to [17, Theorem 3.2], the optimal solutions \mathbf{X}_q of (54) satisfy $\sum_{q=1}^K \text{rank}^2\{\mathbf{X}_q^*\} \leq K$. Therefore, problem (52) can yield rank-1 optimal \mathbf{X}_q^* 's for an arbitrary K . ■

Algorithm 5 Randomized CHE Max-Min Algorithm

- 1: **Initialize** Set $l = 0$; initialize $\{\mathbf{p}_q^{(0)}\}_{q=1}^K$; update $\{\mathbf{t}_q^{(0)}\}_{q=1}^K$ by (37c); update \bar{c}'_q , $\mathbf{C}'_{q,1}$ and $\mathbf{A}'_{q,1}$ by (50), (39) and (40), respectively; update $-\gamma_2^{(0)} = \max_q \text{Tr}\{\mathbf{A}'_{q,1} \mathbf{p}_q^{(0)} [\mathbf{p}_q^{(0)}]^H\} + \bar{c}'_q$;
 - 2: **repeat**
 - 3: $l = l + 1$;
 - 4: For $q = 1, \dots, K$, update \bar{c}'_q , $\mathbf{C}'_{q,1}$ and $\mathbf{A}'_{q,1}$ with $\mathbf{t}_q^{(l-1)}$ by (50), (39) and (40), respectively; Solve problem (52) by the interior-point method, yielding high-rank $\mathbf{X}_q^* \forall q$;
 - 5: Find the optimal $q^* \triangleq q_0 = \arg \max_q \text{Tr}\{\mathbf{A}'_{q,1} \mathbf{X}_q^*\} + \bar{c}'_q$; update $\mathbf{B}_{1,q}$ and $\mathbf{B}_{2,q} \forall q$ for problem (55);
 - 6: Compute $\mathbf{Q}_q \triangleq \mathbf{U}_q^H \mathbf{X}_q^{*1/2} \mathbf{B}_{2,q} \mathbf{X}_q^{*1/2} \mathbf{U}_q \forall q$; input \mathbf{Q}_q into [18, Algorithm 3], yielding *randomized* \mathbf{v}_q ; update $\mathbf{p}_q^{(l)} = \mathbf{X}_q^{*1/2} \mathbf{U}_q \mathbf{v}_q$ according to Theorem 5.
 - 7: Update $-\gamma_2^{(l)} = \max_q \text{Tr}\{\mathbf{A}'_{q,1} \mathbf{p}_q^{(l)} [\mathbf{p}_q^{(l)}]^H\} + \bar{c}'_q$;
 - 8: **until** $|\gamma_2^{(l)} - (-\gamma_2^{(l-1)})| / |\gamma_2^{(l)}| \leq \epsilon$
 - 9: $\bar{\mathbf{s}}_n^* = \sum_{q=1}^K [\mathbf{p}_q^{(l)}]_{n,1} \mathbf{h}_{q,n}^* / \sqrt{M}$ and $\mathbf{s}_{\text{asym}}^* = \sqrt{E/M} \bar{\mathbf{s}}_n^*$.
-

1) *CHE Max-Min Algorithm with Rank Reduction (RR):* In order to solve (51) iteratively and finally achieve a stationary point of (49), we propose an algorithm similar to Algorithm 4, where the RR procedure is exploited to obtain the rank-1 optimal solution $\bar{\mathbf{X}}_q$ for (52). Specifically, at each iteration l , $\mathbf{A}'_{q,1}$ and \bar{c}'_q are updated for the l th AP (52). Exploiting the interior-point algorithm to solve (52) achieves high-rank \mathbf{X}_q^* . Obtaining the optimal $q^* \triangleq q_0 = \arg \max_q \text{Tr}\{\mathbf{A}'_{q,1} \mathbf{X}_q^*\} + \bar{c}'_q$, problem (54) can be formulated. Applying the RR [17, Algorithm 1] to (54) yields rank-1 solutions. As the RR procedure is deterministic, solving (52) (and yielding rank-1 solutions) iteratively achieves a stationary point of (49). Due to space constraint, the algorithm is not outlined in pseudocode.

2) *Randomized CHE Max-Min Algorithm:* In the above algorithm, the rank-1 solution of (54) is achieved by an iterative RR procedure. The following Theorem 5 then reveals that such a rank-1 solution can also be found by *one* randomized step. Based on this, we propose a randomized CHE max-min algorithm. In the following, for notational simplicity, $\mathbf{A}'_{q,1}$ (for $q \neq q_0$), $-\mathbf{A}'_{q_0,1}$ and $\Lambda_q \mathbf{I}$ in (54) are respectively designated as $\mathbf{B}_{1,q}$, \mathbf{B}_{1,q_0} and $\mathbf{B}_{2,q}$, such that (54) can be recast as

$$\min_{\{\mathbf{X}_q \succeq 0\}_{q=1}^K} -\text{Tr}\{\mathbf{B}_{1,q_0} \mathbf{X}_{q_0}\} \quad (55a)$$

$$\text{s.t. } \text{Tr}\{\mathbf{B}_{1,q} \mathbf{X}_q\} + \text{Tr}\{\mathbf{B}_{1,q_0} \mathbf{X}_q\} \leq \bar{c}'_{q_0} - \bar{c}'_q, \forall q \neq q_0, \quad (55b)$$

$$\sum_{q=1}^K \text{Tr}\{\mathbf{B}_{2,q} \mathbf{X}_q\} = 1. \quad (55c)$$

Theorem 5: Suppose that $\{\mathbf{X}_q^*\}_{q=1}^K$ are the high-rank optimal solutions of problem (55). Denote $\mathbf{X}_q^{*1/2}$ as the Hermitian square root matrix of $\mathbf{X}_q^* = \mathbf{X}_q^{*1/2} \mathbf{X}_q^{*1/2}$ and perform the EVD $\mathbf{X}_q^{*1/2} \mathbf{B}_{1,q} \mathbf{X}_q^{*1/2} = \mathbf{U}_q \Sigma_q \mathbf{U}_q^H$. Then, there are randomized vectors $\mathbf{v}_q \in \mathbb{C}^N \forall q$, such that the rank-1 matrices $\mathbf{X}_{q,r1} = \mathbf{x}_{q,r1} \mathbf{x}_{q,r1}^H$ (where $\mathbf{x}_{q,r1} \triangleq \mathbf{X}_q^{*1/2} \mathbf{U}_q \mathbf{v}_q$) are the globally optimal solutions of (55).

Proof: See Appendix D for details. ■

Based on Theorem 5, the randomized algorithm is proposed as Algorithm 5. Note that the stopping criterion at Line 8 of Algorithm 5 is different from that in Algorithm 3 and designed based on the convergence of the objective function. This is due to the fact that the randomized \mathbf{v}_q make the minimizers

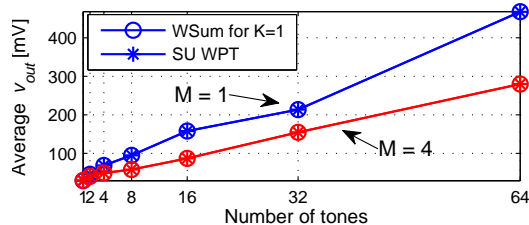


Fig. 3. Average v_{out} as a function of number of sinewaves.

$\{\mathbf{p}_q^{(l)}\}_{l=1}^{\infty} \forall q$ fail to converge to limit points. Therefore, in contrast to the CHE max-min Algorithm with RR, Algorithm 5 may not converge to a stationary point of (49).

VI. PERFORMANCE EVALUATIONS

The simulations consider a typical large open space indoor (or outdoor) WiFi-like environment at a central frequency of 2.4 GHz with 10 MHz bandwidth and uncorrelated spatial domain channels. The power delay profile of the TGN NLOS channel model E [28] is used to generate the frequency-selective fading channel. EIRP at BS is fixed as 36 dBm. The pass loss (used as large-scale fading Λ_q) is computed following [28], and $\Lambda_q = 60.046 \text{ dB} \forall q$, unless otherwise stated.

In the following, the proposed Algorithm 1, Algorithm 2, simplified weighted sum v_{out} maximization algorithm in Section IV-B, Algorithm 3, Algorithm 4, max-min algorithm with randomization in Section V-A2, channel hardening-exploiting (CHE) max-min algorithm with rank reduction in Section V-B1 and Algorithm 5 are referred to as SU WPT, WSum, WSum-S, CHE WSum, Max-Min-RR, Max-Min-Rand, CHE Max-Min-RR and Randomized CHE Max-Min, respectively.

A. Performance of the Weighted Sum Algorithms

Fig. 3 compares the average v_{out} performance of SU WPT and WSum, in the presence of a single user (i.e. $K = 1$). Recall the discussion in Section IV-A that WSum optimizes both the normalized spatial domain beamforming and the power allocation across frequencies, while SU WPT only optimizes the latter. As shown in the plot, SU WPT achieves the same performance as WSum. This confirms Theorem 1 that the optimal spatial domain beamforming is essentially MRC. Note that as EIRP (i.e. the product MP) is fixed, the average v_{out} of $M = 4$ is lower than that of $M = 1$.

We then study the v_{out} performance of SU WPT and CHE WSum, for $K = 1$. We also consider two baseline schemes: uniform power (UP) allocation and adaptive single sinewave (ASS) [4], both of which use MRC as the normalized spatial domain beamforming. UP uniformly allocates power across frequencies, while ASS allocates power to the frequency with respect to the highest channel power gain. It means that UP does not perform frequency domain power optimization, while ASS is optimal for maximizing the v_{out} formulated as a linear model (or 2nd-order truncation model [4], [9], [12]), which is the term in (11) with respect to β_2 . Fig. 4 shows that given M , the performance gain achieved by SU WPT over ASS scales with N and becomes significantly large. This further confirms [4]. The phenomenon is due to that with a fixed bandwidth, as N increases, adjacent frequency domain channel power gains

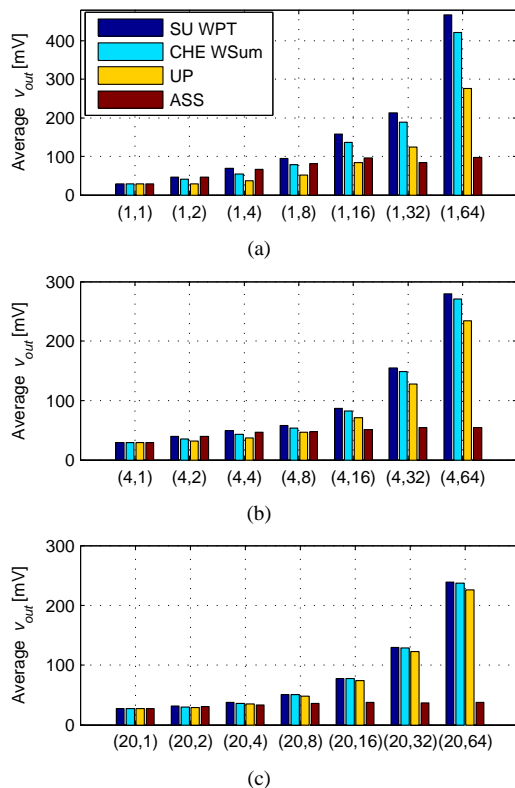


Fig. 4. Average v_{out} as a function of (M, N) with $K = 1$.

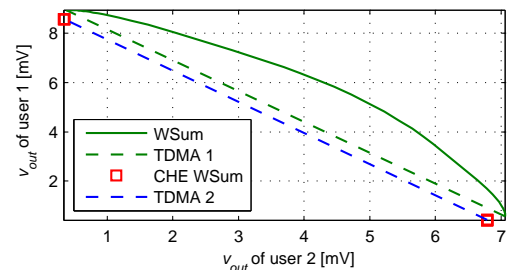


Fig. 5. Achievable v_{out} region, with $M = 20$ and $N = 10$.

are more likely to be distributed within a narrower range. Hence, allocating all the power to the strongest frequency domain channel can be strictly suboptimal. The observation also highlights the inaccuracy of modeling a rectifier as a linear model. Fig. 4 also shows that CHE WSum can offer similar performance to SU WPT for sufficiently large M , while CHE WSum can be performed less frequently due to the optimization in CHE WSum exploiting CSIT only on large-scale fading, which usually varies slowly. We also observe that given M , the performance gain of CHE WSum over UP scales with N . It indicates that the frequency domain power optimization in CHE WSum can benefit from increasing N . This also suggests that the scaling law of WPT [4] offers a lower bound.

We then investigate the achievable v_{out} region of a two-user system, where $\Lambda_1 = \Lambda_2 = 66.07 \text{ dB}$ (corresponding to a distance of 20m). The achievable regions of WSum and CHE WSum are obtained by performing the corresponding algorithm for a given channel realization with various user weight pairs (w_1, w_2) . In the legend of Fig. 5, TDMA 1 (or

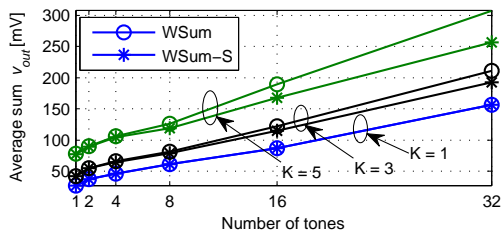


Fig. 6. Average sum v_{out} as a function of N , with $M = 4$.

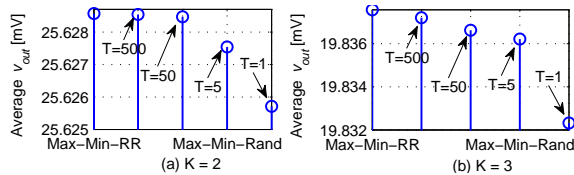


Fig. 7. Average minimum v_{out} of Max-Min-RR and Max-Min-Rand in the presence of two users and three users, with $M = 4$ and $N = 4$.

TDMA 2) means running WSum (or CHE WSum) for each user in a time division manner. Fig. 5 demonstrates that the achievable region of WSum is larger than that of TDMA 1. This is due to WSum performing a tradeoff between the achievable v_{out} of the two users. It is also shown that TDMA 2 is outperformed by TDMA 1. This comes from the fact that TDMA 2 does not exploit the small-scale fading CSI for power optimization across frequencies and users. Note that CHE WSum only obtains two v_{out} pairs. This is explained as follows. CHE WSum is essentially a function of Λ_q and w_q . For $\Lambda_1 = \Lambda_2$, the solution provided by CHE WSum only relies on (w_1, w_2) . When $w_1 \neq w_2$, all the power is always allocated to \mathbf{p}_q^* with $q^* = \arg \max_q w_q$. This is equivalent to the TDMA scenario where only one user is served. On the other hand, when $w_1 = w_2$, all the power is randomly allocated to either \mathbf{p}_1 or \mathbf{p}_2 .

In Fig. 6, WSum is compared to WSum-S in terms of the average v_{out} performance. In the simulations, the weight for each user is set as $w_q = 1$. Recall the discussion in Section IV-B that WSum-S essentially performs optimization in the frequency domain, while fixes the spatial domain beamforming \mathbf{w}_n as the dominant eigenvector of $\sum_{q=1}^K w_q \mathbf{h}_{q,n}^* \mathbf{h}_{q,n}^T$. Intuitively, for $K = 1$, \mathbf{w}_n satisfies Theorem 1. Therefore WSum-S should be equivalent to SU WPT and offer the same performance as WSum. Motivated by this intuition, we plot WSum and WSum-S for $K = 1$ in Fig. 6, and the observation confirms the intuition. Additionally, it is shown that given $K > 1$, the performance gap between WSum and WSum-S increases as N increases, while the gap is negligible in the presence of a small N . Given N , the gap can also scale with K . The above observation highlights the inefficiency of a multiuser design (even partially) based on the linear model. It also suggests that for small K and small N , the less complex WSum-S can yield nearly the same v_{out} performance as WSum.

B. Performance of the Max-Min Algorithms

We first study the average minimum v_{out} performance of Max-Min-Rand, comparing it to that of Max-Min-RR, when $K \leq 3$. Fig. 7 illustrates that Max-Min-RR always outperforms Max-Min-Rand. This is because Max-Min-RR

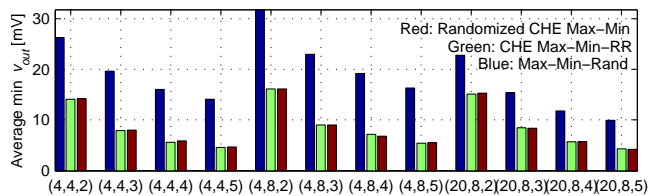


Fig. 8. Average minimum v_{out} as a function of (M, N, K) .

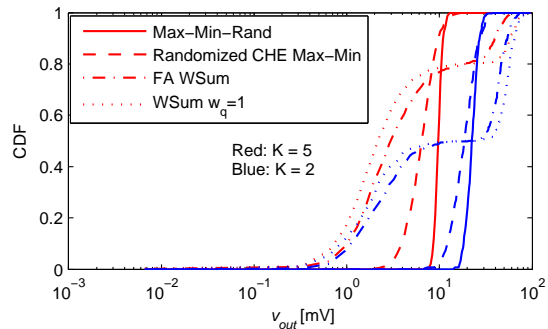


Fig. 9. CDF of v_{out} , with $M = 20$ and $N = 8$.

converges to a stationary point of (43), as discussed in Section V-A1. Despite this, the average minimum v_{out} obtained by Max-Min-Rand is close to that of Max-Min-RR. This results from the high-rank solution \mathbf{X}^* provided by Max-Min-Rand having a dominant eigenvalue which is much larger than the other eigenvalues. As discussed in Section V-A2, the solution of Max-Min-Rand is chosen from T random feasible solutions. It is shown in Fig. 7 that the average minimum v_{out} of Max-Min-Rand scales with T . In the following simulations, we set $T = 50$.

Fig. 8 studies the minimum v_{out} performance of Randomized CHE Max-Min, CHE Max-Min-RR and Max-Min-Rand. As discussed in Section V-B, CHE Max-Min-RR converges to a stationary point of (49), while the minimizers of Randomized CHE Max-Min cannot even converge to a limit point. Intuitively, CHE Max-Min-RR is more likely to outperform Randomized CHE Max-Min in terms of the minimum v_{out} . Nevertheless, Fig. 8 reveals that CHE Max-Min-RR and Randomized CHE Max-Min offer similar performance. Due to this and the fact that Randomized CHE Max-Min computes the rank-1 solution of (54) by one randomized step, Randomized CHE Max-Min is more efficient than CHE Max-Min-RR. Furthermore, the comparison of the average minimum v_{out} with $(M, N) = (4, 4)$ and that with $(M, N) = (4, 8)$ shows that increasing N benefits the max-min algorithms, in terms of the average minimum v_{out} . Fig. 8 shows that given (N, K) , the performance gap between Max-Min-Rand and the CHE max-min algorithms (including CHE Max-Min-RR and Randomized CHE Max-Min) decreases, as M increases. This implies that the CHE Max-Min algorithms and Max-Min-Rand can offer similar performance, when M is sufficiently large. Due to this and lower complexity, Randomized CHE Max-Min would be preferred for large-scale designs.

We now study the CDF performance of Max-Min-Rand and Randomized CHE Max-Min, considering WSum with $w_q = 1 \forall q$ as a baseline scheme. We also consider a fairness-aware (FA) WSum algorithm as another baseline. Intuitively,

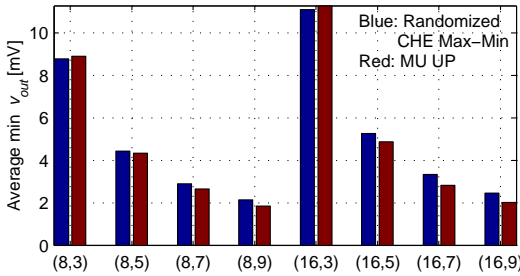


Fig. 10. Average minimum v_{out} as a function of (N, K) , with $M = 50$.

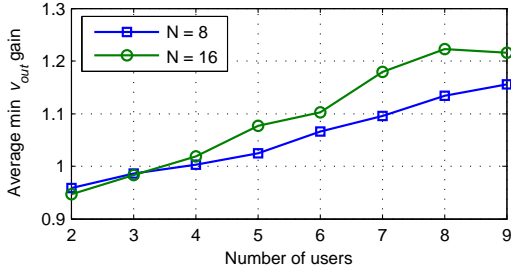


Fig. 11. Average minimum v_{out} gain of Randomized CHE Max-Min over MU UP as a function of K , with $M = 50$.

the larger weights in FA WSum should be assigned to the users suffering from lower channel power gains. Due to the fact that v_{out} is also a nonlinear function of spatial/frequency domain channel gains (for given transmit waveforms), an indicator is designed to jointly evaluate user q 's spatial and frequency domain channels. Specifically, assume that only user q is served, the output voltage achieved by UP (i.e. the baseline in Fig. 4) is exploited as the indicator for user q and designated as α_q . Therefore, the fairness-aware weight $w_q = \alpha_q^{-1} / (\sum_{q=1}^K \alpha_q^{-1})$. Fig. 9 demonstrates that Max-Min-Rand outperforms other algorithms in terms of fairness. Numerical results also confirm that FA WSum offers fairer v_{out} than WSum. It is worth noting that although the optimization in Randomized CHE Max-Min could not leverage CSIT on small-scale fading, the algorithm still demonstrates better fairness than FA WSum.

We then investigate the average minimum v_{out} performance of Randomized CHE Max-Min, considering larger M and N . The baseline is a multi-user (MU) uniform power (UP) allocation scheme, which exploits the asymptotically optimal spatial domain beamforming and uniformly allocates the transmit power across frequencies and users, such that the precoder at frequency n is $\mathbf{s}_n = \sqrt{P} \mathbf{w}_n / \sqrt{\sum \|\mathbf{w}_n\|^2}$ for $\mathbf{w}_n = \sum_{q=1}^K \mathbf{h}_{q,n}^* / \|\mathbf{h}_{q,n}\|$. In contrast, Randomized CHE Max-Min not only allocates more power to the \mathbf{p}_q corresponding to a lower Λ_q , but also optimizes power allocation across frequencies, such that all the users achieve the same asymptotical output voltage. In the simulations of Figs. 10 and 11, Randomized CHE Max-Min uniformly allocates power across users, due to the same $\Lambda_q \forall q$. Fig. 10 shows that when K is small, as channel fluctuations contribute to v_{out} , Randomized CHE Max-Min can be outperformed by MU UP. As K increases, Randomized CHE Max-Min can outperform MU UP, thanks to the power allocation optimization across frequencies. In Fig. 10, the comparison of data with respect to $N = 8$ and that with respect to $N = 16$ indicates that

increasing N improves the average minimum v_{out} . Fig. 11 presents the average minimum v_{out} gain of Randomized CHE Max-Min over MU UP, for $N = 8$ and $N = 16$. It is shown that the curve of $N = 16$ is higher than that of $N = 8$ when K is sufficiently large, and the gap between the two curves increases. This can be explained by the fact that the frequency domain power optimization in CHE Max-Min is a nonlinear model-based design, and it benefits from increasing N .

VII. CONCLUSIONS

This paper studies waveform optimizations for the large-scale multi-antenna multi-sine wireless power transfer (WPT). We have developed an optimization framework towards low-complexity algorithms for the problems involving the nonlinear rectenna model. Multiuser algorithms are designed to maximize the weighted-sum/minimum rectenna output DC voltage. The study highlights the effect of the nonlinearity on the waveform design. It is revealed that the single-user WPT design boils down to optimizing power allocation across frequencies. However, in general, to maximize the weighted-sum criterion, the optimal spatial domain beamforming and the optimal frequency domain power allocation cannot be designed separately. In the presence of a larger number of antennas and sinewaves, channel hardening-exploiting algorithms are designed as well. Asymptotic analysis reveals that the structure of the asymptotical optimal spatial domain precoder can be designed prior to the power allocation optimization across users and frequencies. Numerical results confirm the inefficiency of the linear model-based multiuser waveform design. It is also shown that accounting for the nonlinear model, the proposed multiuser algorithms can benefit from the increasing number of sinewaves, in terms of the output voltage performance.

APPENDIX

A. Proof of Theorem 1

To prove Theorem 1, we show that given fixed $\xi_n^* \forall n$, $\tilde{\mathbf{s}}_n^*$ has to be MRC, such that (10) can be maximized. It can be easily seen that to maximize $f_{\text{LPF}}(y_1^2(t))$ i.e. $\sum_{n=1}^N \mathbf{s}_n^H \mathbf{h}_{1,n}^* \mathbf{h}_{1,n}^T \mathbf{s}_n$, the optimal $\tilde{\mathbf{s}}_n^* = e^{j\phi_n} \mathbf{h}_{1,n}^* / \|\mathbf{h}_{1,n}\|$; otherwise another $\tilde{\mathbf{s}}_n^*$ can always be found, yielding a higher value. Then, we will show that this $\tilde{\mathbf{s}}_n^*$ also maximizes $f_{\text{LPF}}(y_1^4(t))$.

Given n_1, n_2, n_3 and n_4 , as the value of $\mathbf{s}_{n_3}^H \mathbf{h}_{1,n_3}^* \mathbf{h}_{1,n_1}^T \cdot \mathbf{s}_{n_1}^H \mathbf{h}_{1,n_4}^* \mathbf{h}_{1,n_2}^T \mathbf{s}_{n_2}$ is equal to that of $(\mathbf{s}_{n_2}^H \mathbf{h}_{1,n_2}^* \mathbf{h}_{1,n_4}^T \cdot \mathbf{s}_{n_1}^H \mathbf{h}_{1,n_1}^* \mathbf{h}_{1,n_3}^T \mathbf{s}_{n_3})^*$, (9c) can be written as

$$f_{\text{LPF}}(y_1^4(t)) = \frac{3}{2} \sum \text{Re} \{ \mathbf{s}_{n_3}^H \mathbf{h}_{1,n_3}^* \mathbf{h}_{1,n_1}^T \mathbf{s}_{n_1}^H \mathbf{h}_{1,n_4}^* \mathbf{h}_{1,n_2}^T \mathbf{s}_{n_2} \}, \quad (\text{A.1})$$

where $n_1, n_2, n_3, n_4 \in \{1, \dots, N\}$ and $n_1 + n_2 = n_3 + n_4$. Note that although the value of $\mathbf{s}_{n_3}^H \mathbf{h}_{1,n_3}^* \mathbf{h}_{1,n_1}^T \mathbf{s}_{n_1}^H \mathbf{h}_{1,n_4}^* \mathbf{h}_{1,n_2}^T \mathbf{s}_{n_2}$ is generally complex, this value has to be real in order to maximize $f_{\text{LPF}}(y_1^4(t))$, due to $\text{Re}\{\cdot\}$ in (A.1). In the following, we first show the optimality of $\tilde{\mathbf{s}}_{n_3}^*$ and $\tilde{\mathbf{s}}_{n_2}^*$, with given $\mathbf{s}_{n_1}^*$ and $\mathbf{s}_{n_4}^*$. Specifically, defining $\tilde{\mathbf{s}}_n^* = e^{j\phi_n} \tilde{\mathbf{w}}_n^*$, we shall show the optimal $\tilde{\mathbf{w}}_n^* = \mathbf{h}_{1,n}^* / \|\mathbf{h}_{1,n}\|$ for $n \in \{n_2, n_3\}$. Without loss of generality, assuming $\mathbf{h}_{1,n_1}^T \mathbf{s}_{n_1}^* [\mathbf{s}_{n_4}^*]^H \mathbf{h}_{1,n_4}^* = c_{n_1, n_4} \in \mathbb{C}$, with the structure of \mathbf{s}_n^* shown in Theorem 1,

$[\mathbf{s}_{n_3}^*]^H \mathbf{h}_{1,n_3}^* \mathbf{h}_{1,n_1}^T \mathbf{s}_{n_1}^* [\mathbf{s}_{n_4}^*]^H \mathbf{h}_{1,n_4}^* \mathbf{h}_{1,n_2}^T \mathbf{s}_{n_2}^*$ can be written as $[\mathbf{s}_{n_3}^*]^* e^{-j\phi_{n_3}} [\tilde{\mathbf{w}}_{n_3}^*]^H \mathbf{h}_{1,n_3}^* c_{n_1,n_4} \mathbf{h}_{1,n_2}^T \xi_{n_2}^* e^{j\phi_{n_2}} \tilde{\mathbf{w}}_{n_2}^*$. To maximize $\text{Re}\{[\mathbf{s}_{n_3}^*]^* e^{j(\phi_{n_2}-\phi_{n_3})} [\tilde{\mathbf{w}}_{n_3}^*]^H \mathbf{h}_{1,n_3}^* \mathbf{h}_{1,n_2}^T \tilde{\mathbf{w}}_{n_2}^* \xi_{n_2}^* c_{n_1,n_4}\}$, $\tilde{\mathbf{w}}_{n_3}^*$ and $\tilde{\mathbf{w}}_{n_2}^*$ turn out to be $\mathbf{h}_{n_3}^*/\|\mathbf{h}_{n_3}\|$ and $\mathbf{h}_{n_2}^*/\|\mathbf{h}_{n_2}\|$, which are the left and the right singular vectors of the rank-1 matrix $\mathbf{h}_{1,n_3}^* \mathbf{h}_{1,n_2}^T$. Meanwhile, the value of $\phi_{n_2}-\phi_{n_3}$ should be determined such that $[\mathbf{s}_{n_3}^*]^* \xi_{n_2}^* c_{n_1,n_4} e^{j(\phi_{n_2}-\phi_{n_3})}$ is real. Similarly, given $\mathbf{s}_{n_2}^*$ and $\mathbf{s}_{n_3}^*$, $[\mathbf{s}_{n_3}^*]^H \mathbf{h}_{1,n_3}^* \mathbf{h}_{1,n_1}^T \mathbf{s}_{n_1}^* [\mathbf{s}_{n_4}^*]^H \cdot \mathbf{h}_{1,n_4}^* \mathbf{h}_{1,n_2}^T \mathbf{s}_{n_2}^*$ becomes $[\mathbf{s}_{n_4}^*]^* e^{j(\phi_{n_1}-\phi_{n_4})} [\tilde{\mathbf{w}}_{n_4}^*]^H \mathbf{h}_{1,n_4}^* c_{n_2,n_3} \cdot \mathbf{h}_{1,n_1}^T \xi_{n_1}^* \tilde{\mathbf{w}}_{n_1}^*$. It can be shown that $\tilde{\mathbf{w}}_{n_1}^* = \mathbf{h}_{n_1}^*/\|\mathbf{h}_{n_1}\|$ and $\tilde{\mathbf{w}}_{n_4}^* = \mathbf{h}_{n_4}^*/\|\mathbf{h}_{n_4}\|$.

B. Proof of Proposition 1

In (22), as $M_0'' > 0$ and $\mathbf{X} \succeq 0$, it follows that $t_0^{(l-1)} \geq 0$. Hence, $\text{Tr}\{\mathbf{A}_1''\} < 0$. This means that \mathbf{A}_1'' always exists an eigenvalue less than zero. Given that problem (21) yields a rank-1 solution $\mathbf{X}^* = \mathbf{x}^*[\mathbf{x}^*]^H$, (21) is equivalent to a non-convex quadratically constrained quadratic problem (QCQP) given by $\min_{\mathbf{x}}\{\mathbf{x}^H \mathbf{A}_1'' \mathbf{x} : \|\mathbf{x}\|^2 \leq P\}$. The KKT conditions of this problem indicates that the stationary points are in the directions of the eigenvectors of \mathbf{A}_1'' . Hence, $\mathbf{x}^* = \sqrt{P}[\mathbf{U}_{\mathbf{A}_1''}]_{\min}$.

C. Proof of Theorem 2

Since $-g(\mathbf{t})$ is convex, $g(\mathbf{t}) \leq \tilde{g}(\mathbf{t}, \mathbf{t}^{(l-1)})$. Therefore, $\tilde{g}(\mathbf{t}^{(l)}, \mathbf{t}^{(l)}) = g(\mathbf{t}^{(l)}) \leq \tilde{g}(\mathbf{t}^{(l)}, \mathbf{t}^{(l-1)})$, which indicates that the optimal solution $\mathbf{X}^{(l-1)}$ of the $(l-1)$ th AP (20) is a feasible point of the l th AP (20). As the AP (20) is convex, the objective functions over iterations satisfy $\gamma_0^{(l)} \leq \gamma_0^{(l-1)}$. Under the assumption of the uniqueness of the eigenvalue decomposition, applying the inequality $\gamma_0^{(l)} \leq \gamma_0^{(l-1)}$, by contradiction [29, Proof of Proposition 2.7.1], we can show that the sequence of the minimizer $\{\gamma_0^{(l)}, \mathbf{t}^{(l)}, \mathbf{X}^{(l)}\}_{l=0}^\infty$ converges to a limit point. As $\nabla g(\mathbf{t}^{(l)}) = \nabla \tilde{g}(\mathbf{t}^{(l)}, \mathbf{t}^{(l)})$, the solution of (20) finally converges to a stationary point of (18). As such a stationary point (with a rank-1 \mathbf{X}^*) is also a stationary point of (17), Algorithm 1 converges to a stationary point of (17).

D. Proof of Theorem 5

It is observed in problem (55) that given a certain q , the optimization variable \mathbf{X}_q is multiplied by $\mathbf{B}_{1,q}$ and $\mathbf{B}_{2,q}$, respectively. This is reminiscent of the application of [18, Lemma 3.3] to the QCQP with two double-sided constraints. Here we prove Theorem 5 by [18, Lemma 3.3]: there always exists a randomized \mathbf{v}_q (for $q \in \{1, \dots, K\}$), such that $\text{Tr}\{\mathbf{B}_{1,q} \mathbf{X}_{q,r1}\} = \text{Tr}\{\mathbf{B}_{1,q} \mathbf{X}_q^{*1/2} \mathbf{U}_q \mathbf{v}_q \mathbf{v}_q^H \mathbf{U}_q^H \mathbf{X}_q^{*1/2}\} = \text{Tr}\{\Sigma_q \mathbf{v}_q \mathbf{v}_q^H\} = \text{Tr}\{\Sigma_q \mathbf{I}\} = \text{Tr}\{\mathbf{B}_{1,q} \mathbf{X}_q^*\}$. Meanwhile, $\text{Tr}\{\mathbf{B}_{2,q} \mathbf{X}_{q,r1}\} = \text{Tr}\{\mathbf{B}_{2,q} \mathbf{X}_q^{*1/2} \mathbf{U}_q \mathbf{v}_q \mathbf{v}_q^H \mathbf{U}_q^H \mathbf{X}_q^{*1/2}\} = \text{Tr}\{\mathbf{U}_q^H \mathbf{X}_q^{*1/2} \mathbf{B}_{2,q} \mathbf{X}_q^{*1/2} \mathbf{U}_q \mathbf{v}_q \mathbf{v}_q^H\} = \text{Tr}\{\mathbf{U}_q^H \mathbf{X}_q^{*1/2} \mathbf{B}_{2,q} \cdot \mathbf{X}_q^{*1/2} \mathbf{U}_q \mathbf{I}\} = \text{Tr}\{\mathbf{B}_{2,q} \mathbf{X}_q^*\}$.

REFERENCES

[1] Y. Huang and B. Clerckx, "Waveform optimization for large-scale multi-antenna multi-sine wireless power transfer," in *IEEE International Workshop on Signal Processing Advances in Wireless Communications 2015*, Jul. 2016.

[2] A. Costanzo and D. Masotti, "Smart solutions in smart spaces: Getting the most from far-field wireless power transfer," *IEEE Microw. Mag.*, vol. 17, no. 5, pp. 30–45, May 2016.

[3] A. Boaventura et al., "Boosting the efficiency: Unconventional waveform design for efficient wireless power transfer," *IEEE Microw. Mag.*, vol. 16, no. 3, pp. 87–96, Apr. 2015.

[4] B. Clerckx and E. Bayguzina, "Waveform design for wireless power transfer," accepted to *IEEE Transactions on Signal Processing*, available online at arXiv: 1604.00074.

[5] Y. Zeng and R. Zhang, "Optimized training design for wireless energy transfer," *IEEE Trans. Commun.*, vol. 63, no. 2, pp. 536–550, Feb. 2015.

[6] J. Xu and R. Zhang, "Energy beamforming with one-bit feedback," *IEEE Trans. Signal Process.*, vol. 62, no. 20, pp. 5370–5381, Oct. 2014.

[7] S. Ladan and K. Wu, "Nonlinear modeling and harmonic recycling of millimeter-wave rectifier circuit," *IEEE Trans. Microw. Theory Tech.*, vol. 63, no. 3, pp. 937–944, Mar. 2015.

[8] C. R. Valenta, M. M. Morys, and G. D. Durgin, "Theoretical energy-conversion efficiency for energy-harvesting circuits under power-optimized waveform excitation," *IEEE Trans. Microw. Theory Tech.*, vol. 63, no. 5, pp. 1758–1767, May 2015.

[9] X. Zhou, R. Zhang, and C. K. Ho, "Wireless information and power transfer: Architecture design and rate-energy tradeoff," *IEEE Trans. Commun.*, vol. 61, no. 11, pp. 4754–4767, Oct. 2013.

[10] A. Boaventura and N. Carvalho, "Maximizing dc power in energy harvesting circuits using multisine excitation," in *2011 IEEE MTT-S International Microwave Symposium Digest*, Jun. 2011.

[11] M. Chiang, "Geometric programming for communication systems," *Foundations and Trends of Communications and Information Theory*, vol. 2, no. 1-2, pp. 1–156, Aug. 2005.

[12] S. Wetenkamp, "Comparison of single diode vs. dual diode detectors for microwave power detection," in *1983 IEEE MTT-S International Microwave Symposium Digest*, May 1983, pp. 361–363.

[13] C. Ling, J. Nie, L. Qi, and Y. Ye, "Biquadratic optimization over unit spheres and semidefinite programming relaxations," *SIAM J. Optim.*

[14] Z.-Q. Luo and S. Zhang, "A semidefinite relaxation scheme for multivariate quartic polynomial optimization with quadratic constraints," *SIAM J. Optim.*, vol. 20, no. 4, pp. 1716–1736, Jan. 2010.

[15] I. M. Bomze, C. Ling, L. Qi, and X. Zhang, "Standard bi-quadratic optimization problems and unconstrained polynomial reformulations," *Journal of Global Optimization*, vol. 52, no. 4, pp. 663–687, Apr. 2012.

[16] B. R. Marks and G. P. Wright, "A general inner approximation algorithm for nonconvex mathematical programs," *Operations Research*, vol. 26, no. 4, pp. 681–683, 1978.

[17] Y. Huang and D. P. Palomar, "Rank-constrained separable semidefinite programming with applications to optimal beamforming," *IEEE Trans. Signal Process.*, vol. 58, no. 2, pp. 664–678, Feb. 2010.

[18] —, "Randomized algorithms for optimal solutions of double-sided QCQP with applications in signal processing," *IEEE Trans. Signal Process.*, vol. 62, no. 5, pp. 1093–1108, Mar. 2014.

[19] J. G. VanAntwerp, R. D. Braatz, and N. V. Sahinidis, "Globally optimal robust process control," *Journal of Process Control*, vol. 9, no. 5, pp. 375–383, 1999.

[20] T. Adah and S. Haykin, *Adaptive Signal Processing: Next Generation Solutions*. Hoboken, New Jersey: John Wiley & Sons, 2010.

[21] A. Ben-Tal and A. Nemirovski, *Lectures on Modern Convex Optimization: Analysis, Algorithms, and Engineering Applications*, ser. MPSIAM Series on Optimization.

[22] B. N. Parlett, "The QR algorithm," *IEEE Comput. Sci. Eng.*, vol. 2, no. 1, pp. 38–42, Jan. 2000.

[23] J. C. Bezdek and R. J. Hathaway, "Convergence of alternating optimization," *Neural, Parallel Sci. Comput.*, vol. 11, no. 4, pp. 351–368, Dec. 2003.

[24] Y. Huang and B. Clerckx, "Relaying strategies for wireless-powered mimo relay networks," 2016, accepted to *IEEE Transactions on Wireless Communications*.

[25] Z. Xiang, M. Tao, and X. Wang, "Massive MIMO multicasting in noncooperative cellular networks," *IEEE J. Sel. Areas Commun.*, vol. 32, no. 6, pp. 1180–1193, Jun. 2014.

[26] J. Dattorro, *Convex Optimization and Euclidean Distance Geometry*. Palo Alto, California: M&B Publishing, 2005, v2014.04.08.

[27] M. Grant and S. Boyd, "CVX: Matlab software for disciplined convex programming, version 2.1," <http://cvxr.com/cvx>, Mar. 2014.

[28] V. Erceg et al, "TGN channel models," in *Version 4. IEEE 802.11-03/940r4*, May 2004.

[29] D. P. Bertsekas, *Nonlinear Programming*, 2nd ed. Belmont, MA: Athena Scientific, 1999.